MATHEMATICS OF COMPUTATION
Volume 89, Number 323, May 2020, Pages 1161–1191
https://doi.org/10.1090/mcom/3497
Article electronically published on January 6, 2020

NUMERICAL INVERSE LAPLACE TRANSFORM FOR CONVECTION-DIFFUSION EQUATIONS

NICOLA GUGLIELMI, MARÍA LÓPEZ-FERNÁNDEZ, AND GIANCARLO NINO

Abstract. In this paper a novel contour integral method is proposed for linear convection-diffusion equations. The method is based on the inversion of the Laplace transform and makes use of a contour given by an elliptic arc joined symmetrically to two half-lines. The trapezoidal rule is the chosen integration method for the numerical inversion of the Laplace transform, due to its well-known fast convergence properties when applied to analytic functions. Error estimates are provided as well as careful indications about the choice of several involved parameters. The method selects the elliptic arc in the integration contour by an algorithmic strategy based on the computation of pseudospectral level sets of the discretized differential operator. In this sense the method is general and can be applied to any linear convection-diffusion equation without knowing any a priori information about its pseudospectral geometry. Numerical experiments performed on the Black–Scholes ($1D$) and Heston ($2D$) equations show that the method is competitive with other contour integral methods available in the literature.

1. Introduction

We consider the time discretization of initial value problems for linear systems of ODEs:

$$\frac{\partial u}{\partial t} = Au + b(t), \qquad u(0) = u_0, \tag{1}$$

for $t > 0$, A a discrete version of an elliptic operator, and b a source term including possibly boundary contributions. The solution u will thus be a time-dependent vector, of dimension equal to the number of degrees of freedom in the spatial semi-discretization of the reference problem. We are particularly interested in equations arising in mathematical finance, such as Black–Scholes, Heston or Heston–Hull–White equations [2, 5, 6].

Classical methods to approximate the solution $u(t)$ to (1) include Runge–Kutta and multistep integrators. Also splitting schemes, like ADI methods, have been proposed to solve the continuous reference problem; see for example [7–10] for the Heston equation. All these methods are of time-stepping type, and thus, in order to approximate the solution at a certain time t_n, approximations at certain smaller times $0 < t_1 < t_2 < \cdots < t_n$ must be previously computed. For large times or high

Received by the editor September 5, 2018, and, in revised form, July 2, 2019, and August 21, 2019.

2010 *Mathematics Subject Classification.* Primary 65L05, 65R10, 65J10, 65M20, 91-08.

Key words and phrases. Contour integral methods, pseudospectra, Laplace transform, numerical inversion of Laplace transform, trapezoidal rule, quadrature for analytic functions.

The first and second authors acknowledge INdAM GNCS for their financial support.

The second author acknowledges partial support of the Spanish grant MTM2016-75465.

accuracy requirements this procedure can be extremely demanding in terms of CPU time. An alternative to time-stepping methods to compute the solution at (a few) given times, large or not, can be derived based on the Laplace transform and its numerical inversion. This approach has been successfully developed in [4, 14, 15, 18] for linear evolutionary problems governed by a *sectorial* operator, this is, assuming that A in (1) has a bounded resolvent outside a certain acute sector in the complex half-plane $\{z \in \mathbb{C} \,|\, \mathrm{Re}(z) \leq \alpha\}$, for some $\alpha \in \mathbb{R}$. The magnitude of the resolvent norm $\left\|(zI - A)^{-1}\right\|$ deeply impacts on the rate of convergence of the method. For this reason, the integration contour must be chosen according to the pseudospectral geometry of A. In particular, if A is nonnormal the pseudospectral geometry of A can be difficult to estimate [20]. The spatial discretization of a convection-diffusion operator typically leads to a nonnormal matrix [11, 17, 22]. In the present paper we propose a novel contour integral method for (1), which includes a preliminary study of the pseudospectral level curves of A.

In what follows we will assume that both the resolvent of A and the Laplace transform of the source term $b(t)$ exist, are available, and admit a bounded analytic extension to a certain sector $\arg z < \pi - \delta$, for some $0 < \delta < \frac{\pi}{2}$. The case of more general sources is out of the scope of the present manuscript but has been considered in the literature [18]. Notice also [13], where the inversion method for the Laplace transform in [15] is used to derive a fast implementation of implicit Runge–Kutta schemes applied to solve (1) at a required final time, allowing for rather general inhomogeneity b. In the present paper we restrict our attention to the direct application of the Laplace transform method to (1) and thus make stronger hypotheses about b. In this way, we can apply the (unilateral) Laplace transform $\mathcal{L} : f \mapsto \hat{f}(z) := \int_0^{+\infty} e^{-zt} f(t)\, dt$ to both the sides of the system in (1), which leads to the following algebraic equation for $\hat{u} = \mathcal{L}(u)$:

$$\hat{u}(z) = (zI - A)^{-1} \left(u_0 + \hat{b}(z)\right), \tag{2}$$

where $\hat{b} = \mathcal{L}(b)$ and I stands for the identity matrix. The inversion formula for the Laplace transform provides the following representation of the unknown function u:

$$u(t) = \frac{1}{2\pi \mathrm{i}} \int_{\mathcal{G}} e^{zt} \hat{u}(z)\, dz, \tag{3}$$

where due to our hypotheses the integration contour $\mathcal{G}$ can be chosen as a deformation of the vertical Bromwich contour, in such a way that it runs from $-\mathrm{i}\infty$ to $+\mathrm{i}\infty$ and lays to the right of the singularities of $\hat{u}$. These are the eigenvalues of A and all possible singularities of $\hat{b}$. The discretization of (3) by some quadrature rule will provide an approximation of $u(t)$, for a given t.

Under similar hypotheses about $\hat{u}(z)$, several authors have proposed different contour profiles and parameterizations for $\mathcal{G}$. The trapezoidal rule has then been applied to discretize the resulting integrals (see, e.g., [21]). Probably the first relevant reference is [19], where the author analyzes a cotangent mapping with horizontal asymptotes. Much more recently, the cotangent contour have been improved in [3]. Alternatively hyperbolic contours have been considered in [4, 14, 15, 18], with a focus on evolutionary problems governed by sectorial operators, whereas in [22] a parabolic profile for $\mathcal{G}$ is chosen. In all these references, the resulting scheme converges with spectral accuracy, with different rates of convergence according to the

particular application and the range of times at which the inverse Laplace transform is required. An application of the parabolic contour to solve precisely Black–Scholes and Heston equations is studied in [11]. All these methods require in practice some a priori knowledge of the pseudospectral geometry of A. This information is not always analytically available, as is the case of Heston's equation. In the present work we combine a preliminary numerical investigation of the pseudospectral level sets of A with the efficient inversion of the Laplace transform. The shape of the observed pseudospectral level curves leads us to specifically choose the integration contour $\mathcal{G}$ to be a section of an ellipse. Parabolic or hyperbolic contours can also be improved from knowledge of the pseudospectrum of A which implies a recomputation of their parametrization (according to the points outlined in Sections 3–4). Preliminary experimental results and analysis with parabolic contours lead to very similar results to the ones shown in Section 5.

Apart from being able to deal with more general problems than those considered in [11, 15, 22], our new method enjoys the following important advantages:

(1) It provides an approximation within a prescribed target accuracy *tol* by dynamically increasing the number of quadrature points on the integration contour, without changing the integration profile and taking advantage of previous computations. This feature is a novelty of our method compared to the quoted alternatives in the literature, where the integration contour depends on the number of quadrature nodes.
(2) It is able to approximate the solution of (1) uniformly for t belonging to large time windows. A careful analysis of this property has only been provided in [15].
(3) Round-off errors are controlled in a robust and systematic way. A careful analysis of this property has only been provided in [15], although our approach here is different
(4) Like all methods based on the numerical inversion of the Laplace transform to solve (1), our method is highly parallellizable, it provides an approximation of the solution u to (1) at a desired time (or time window) without computing any history, and its performance is not affected by the lack of regularity (in space) of the initial data u_0 in (1).

The article is organized as follows. In Section 2 we describe our integration contour $\mathcal{G}$ and review the error estimate for the trapezoidal rule when applied to exponentially decaying integrands. In Section 3 our new method is fully described and analyzed. In Section 4 we provide details about the practical implementation and the computational cost. In Section 5, after a first illustrative application of the method to a canonical convection-diffusion equation, we test the method on Black–Scholes and Heston equations. In Section 6 we compare our new method with the methods in [11] and [15]. Finally, in Section 7 we extend our algorithm to approximate the solution $u(t)$ for t in a time window $[t_0, t_1]$ by using a unique integration contour.

2. Integration contour and the trapezoidal rule

We propose a contour $\mathcal{G}$ in (3) which is the union of two half-lines connected with an open arc of an ellipse as shown in Figure 1.

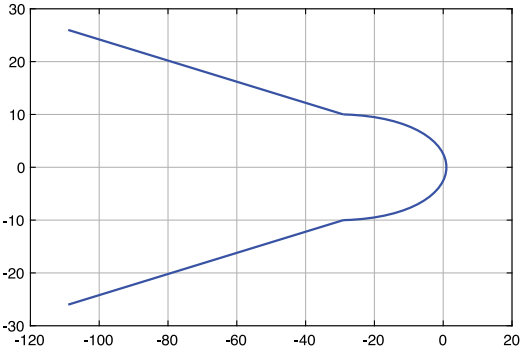

FIGURE 1. Shape of the general integration profile $\mathcal{G}$

In particular, $\mathcal{G}$ is defined as $\{z(x) : x \in (-\infty, \infty)\}$, with

$$z(x) = \begin{cases} \ell_1(x), & x \in \left[-\infty, -\frac{\pi}{2}\right], \\ \Gamma(x), & x \in \left[-\frac{\pi}{2}, \frac{\pi}{2}\right], \\ \ell_2(x), & x \in \left[\frac{\pi}{2}, +\infty\right], \end{cases} \tag{4}$$

where, for constant parameters A_1, A_2, A_3 to be determined,

$$\Gamma(x) = A_1 \cos x + \mathrm{i} A_2 \sin x + A_3$$

parametrizes the elliptic arc and

$$\ell_1(x) = A_3 + x + \frac{\pi}{2} - \mathrm{i}\left(A_2 - d\left(x + \frac{\pi}{2}\right)\right), \quad \ell_2(x) = A_3 - x + \frac{\pi}{2} + \mathrm{i}\left(A_2 + d\left(x - \frac{\pi}{2}\right)\right)$$

parametrize the half-lines.

We recall that the constants in the parametrization must be chosen so that the resulting contour $\mathcal{G}$ leaves to its left the spectrum of A and the singularities of $\hat{b}$. There is quite some freedom in the choice of the two half-lines, as long as their real part goes to minus infinity as $z \to \infty$. Actually, the contribution of the half-lines to the contour integral is expected to be small and will be neglected in practice, as we explain in Subsection 3.3.

We will apply the classical trapezoidal rule to approximate (3), after parametrization by (4). This leads to approximate an integral of the form

$$I = \int_{-\xi}^{\xi} F(x)\, dx, \tag{5}$$

for some $0 < \xi < \pi/2$ and with F satisfying the properties listed in Assumption 1 below.

Assumption 1. The complex extension of the integrand function F in (5) satisfies the following properties:

For some $a > 0$

(1) $F(w)$ $(w \in \mathbb{C})$ is analytic and bounded inside the strip $[-\pi/2, \pi/2] \times [-\mathrm{i}a, \mathrm{i}a]$.

(2) $|F(w)| = |F(-\overline{w})|$ inside the strip $[-\pi/2, \pi/2] \times [-\mathrm{i}a, \mathrm{i}a]$.

(3) $\exists \eta_0 > 0$ $(\eta_0 < \xi)$ and $\exists B_\pm > 0$ such that $\forall \eta \le \eta_0$ one has that
$$|F(x \pm \mathrm{i}a)| \le B_\pm \quad \forall x \in [-\xi - \eta, \xi + \eta]\,.$$

(4) For the same η_0 of the previous point, $\exists S_\pm > 0$ such that $\forall \eta \le \eta_0$
$$|F(x \pm \mathrm{i}a)| \le S_\pm \quad \forall x \in \left[-\frac{\pi}{2}, -\xi - \eta\right] \cup \left[\xi + \eta, \frac{\pi}{2}\right]\,.$$

(5) $\forall x \in \mathbb{R}$ such that $|x| \ge \xi$, one has $|F(x)| \le \theta$, for a certain $\theta > 0$.

Under these hypotheses it is possible to prove the following theorem.

Theorem 1. *Consider the integral I in (5), $N \ge 1$, and the discretization of I by the quadrature formula*
$$I_N = \frac{2\xi}{N} \sum_{j=1}^{N-1} F(x_j) \quad \textit{with} \quad x_j = -\xi + j\frac{2\xi}{N}, \quad j = 1, \dots, N-1.$$
Assume that F satisfies Assumption 1 and take $\eta = \xi/N$. Then
$$|I - I_N| \le \frac{2(\xi+\eta)(B_+ + B_-) + 2(\pi/2 - \delta - \xi - \eta)(S_+ + S_-)}{e^{\frac{a\pi N}{\xi}} - 1} + 4\left(\frac{\pi}{2} - \xi + \frac{\eta}{2}\right)\theta + 4\frac{\xi \log 2}{N\pi} \max_{w \in [-a,a]} |F(-\pi/2 + \delta + iw)|\,, \tag{6}$$
with
$$\delta = \pi/2 - (2k+1)\eta - \xi\,, \qquad k = \left\lfloor \left(\frac{\pi}{2} - \xi - \eta\right)\frac{1}{2\eta} \right\rfloor\,. \tag{7}$$

Proof. The proof is a variant of the one in [1, Appendix] and the one in [12].

We consider the rectangle $R = [-\xi - \eta, \xi + \eta] \times [-\mathrm{i}a, \mathrm{i}a]$ and call Γ_1 the union of its horizontal sides, and Γ_2 and Γ_3 its vertical left and right sides, respectively (see Figure 2). Consider the integral
$$\tilde{I} = \int_{-\xi-\eta}^{\xi+\eta} F(x)\,dx\,.$$
We have
$$\left|I - \tilde{I}\right| \le 2\eta\theta\,. \tag{8}$$
On the one hand, for $w \in \mathbb{C}$,
$$g(w) = \begin{cases} -\frac{1}{2}\,, & \mathrm{Im}(w) > 0\,, \\ \frac{1}{2}\,, & \mathrm{Im}(w) \le 0\,, \end{cases}$$
it follows that
$$\tilde{I} = \int_{\partial R} g(w) F(w)\,dw\,.$$

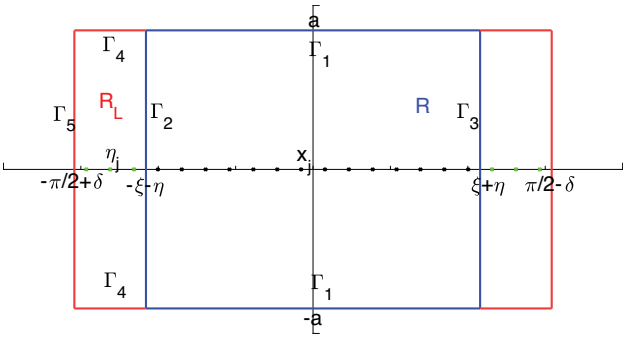

FIGURE 2. The rectangle R

On the other hand, define

$$\tilde{I}_N = \frac{2\xi}{N}\sum_{j=0}^{N} F(x_j)\,, \quad x_j = -\xi + \frac{2\xi j}{N}\,, j = 0,\dots,N\,.$$

One has

$$\left|I_N - \tilde{I}_N\right| \le \frac{4\xi}{N}\theta = 4\eta\theta\,.$$

The function

$$m(w) := \frac{1}{2}\frac{1+e^{-\mathrm{i}\frac{(w+\xi)N\pi}{\xi}}}{1-e^{-\mathrm{i}\frac{(w+\xi)N\pi}{\xi}}}$$

satisfies by the residue theorem

$$\tilde{I}_N = \int_{\partial R} m(w)F(w)\,dw\,.$$

Observe that

$$err_N = |I - I_N| \le \left|I - \tilde{I}\right| + \left|\tilde{I} - \tilde{I}_N\right| + \left|\tilde{I}_N - I_N\right|.$$

Let us consider

$$\tilde{I} - \tilde{I}_N = \int_{\partial R}(g(w)-m(w))\,F(w)\,dw = \left(\int_{\Gamma_1} + \int_{\Gamma_3} - \int_{\Gamma_2}\right)\left[(g(w)-m(w))\,F(w)\right]\,dw\,.$$

We estimate

$$\left|\int_{\Gamma_1}(g(w)-m(w))\,F(w)\,dw\right| \le \frac{2(\xi+\eta)\,(B_+ + B_-)}{e^{\frac{a\pi N}{\xi}}-1}\,. \tag{9}$$

We estimate the integrals over Γ_2, Γ_3. Take the rectangle $R^L = [-\pi/2+\delta, -\xi-\eta]\times[-\mathrm{i}a, \mathrm{i}a]$ and call Γ_5 its left vertical side and Γ_4 the union of its horizontal sides. We define δ as in the statement of the theorem, so that $[-\pi/2+\delta, -\xi-\eta]$ is the largest segment with length an even multiple of η. We have that

$$err_N^L := \int_{-\frac{\pi}{2}+\delta}^{-\xi-\eta} F(x)\,dx - \frac{2\xi}{N}\sum_{j=1}^{k} F(\eta_j) = \int_{\partial R_L}(g(w)-m(w))\,F(w)\,dw\,,$$

with $\eta_j = -\xi - \frac{2\xi j}{N}$, $j = 1, \dots, k$. In other words, err_N^L is the error of the same trapezoidal quadrature rule applied on the integral on the interval $[-\pi/2+\delta, -\xi-\eta]$ with the same spacing $2\xi/N$. In this way, we get

$$\int_{\Gamma_2} (g(w) - m(w))\, F(w)\, dw = err_N^L + \left(-\int_{\Gamma_4} + \int_{\Gamma_5} \right) [(g(w) - m(w))\, F(w)\, dw] \,.$$

On the one hand, we estimate (with $w = x + \mathrm{i}y$)

$$\left| \int_{\Gamma_4} (g(w) - m(w))\, F(w)\, dw \right| \le \frac{(\pi/2 - \delta - \xi - \eta)\,(S_+ + S_-)}{e^{\frac{a\pi N}{\xi}} - 1} \,. \tag{10}$$

On the other hand, we estimate

$$\begin{aligned} &\left| \int_{\Gamma_5} (g(w) - m(w))\, F(w)\, dw \right| \\ &\quad \le \int_{-a}^{a} |(g(-\pi/2 + \delta + \mathrm{i}y) - m(-\pi/2 + \delta + \mathrm{i}y))\, F(-\pi/2 + \delta + \mathrm{i}y)\, dy| \\ &\quad \le \max_{y \in [-a,a]} |F(-\pi/2 + \delta + \mathrm{i}y)| \int_{-a}^{a} |g(-\pi/2 + \delta + \mathrm{i}y) - m(-\pi/2 + \delta + \mathrm{i}y)|\, dy \end{aligned}$$

and

$$\begin{aligned} \int_{-a}^{a} |g(-\pi/2 + \delta + \mathrm{i}y) - m(-\pi/2 + \delta + \mathrm{i}y)|\, dy &= 2 \int_0^a \frac{1}{1 + e^{\frac{\pi w N}{\xi}}}\, dy \\ &\le 2 \int_0^{+\infty} \frac{1}{1 + e^{\frac{\pi w N}{\xi}}}\, dy = \frac{2 \log 2}{\pi} \frac{\xi}{N} \,, \end{aligned}$$

so that

$$\left| \int_{\Gamma_5} (g(w) - m(w))\, F(w)\, dw \right| \le \max_{y \in [-a,a]} |F(-\pi/2 + \delta + \mathrm{i}y)|\, \frac{2 \log 2}{\pi} \frac{\xi}{N} \,. \tag{11}$$

We finally obtain

$$\begin{aligned} \left| err_N^L \right| &= \left| \int_{-\frac{\pi}{2}+\delta}^{-\xi-\eta} F(x)\, dx - \frac{2\xi}{N} \sum_{j=1}^{k} F(\eta_j) \right| \\ &\le \int_{-\frac{\pi}{2}+\delta}^{-\xi-\eta} |F(x)|\, dx + \frac{2\xi}{N} \sum_{j=1}^{k} |F(\eta_j)| \le 2\theta \left(\frac{\pi}{2} - \xi - \eta \right) \,. \end{aligned} \tag{12}$$

By point (2) in Assumption 1, the integral over Γ_3 can be estimated in the same way. The combination of estimates (8), (9), (10), (11), and (12) yields the stated result. □

Remark 1. Observe that δ is defined in such a way that the segment $[-\pi/2 + \delta, -\xi]$ is the largest one whose length is an odd multiple of η. This means that $\delta < 2\eta$.

3. A new method

The only portion of the integration contour $\mathcal{G}$ as defined in (4) that we will use in practice is the half ellipse. This elliptical profile is selected by constructing a suitable conformal mapping $z : [-\pi, \pi] \times [-\mathrm{i}a, \mathrm{i}a] \to \mathbb{C}$. This is analogous to what is done in [11, 14, 15], where parabolas or hyperbolas of integration are defined by some conformal mapping. In particular, we want to map horizontal segments onto

ellipses in the complex plane (we will use the right half of these ellipses). Thus we set

$$z(x+iy) = A_1(y)\cos x + iA_2(y)\sin x + A_3(y)\,. \tag{13}$$

We ask (13) to be holomorphic and impose the Cauchy–Riemann equations, getting that A_3 has to be constant and

$$\begin{aligned} A_1(y) &= a_1 e^{y} + a_2 e^{-y}, \\ A_2(y) &= a_2 e^{-y} - a_1 e^{y}, \end{aligned} \tag{14}$$

where a_1, a_2 are constants. The resulting mapping turns out to be entire, since the partial derivatives of both the real and the imaginary parts are everywhere continuous. It is thus invertible and the complex derivative cannot be zero.

The core idea of using the mapping (13) is to let y vary in the segment $[-a, a]$, for a suitable a, while the integrand function

$$G(w) = e^{z(w)t}\left(z(w)I - A\right)^{-1}\left(u_0 + \hat{b}(z(w))\right) z'(w) \tag{15}$$

stays bounded for every $w = x + \mathrm{i}y$, $x \in [-\pi/2, \pi/2]$, $y \in [-a, a]$. In particular, we will use the mapping (13) to efficiently bound the exponential term $e^{z(w)t}$ and the norm of the resolvent $\left(z(w)I - A\right)^{-1}$. We are doing this by constructing two *external* half ellipses Γ_+, Γ_- delimiting the part of the complex plane where the integrand is bounded. The mapping (13) is required to map the segment from $(-\pi/2, -\mathrm{i}a)$ to $(\pi/2, -\mathrm{i}a)$ onto Γ_- and the segment from $(-\pi/2, \mathrm{i}a)$ to $(\pi/2, \mathrm{i}a)$ onto Γ_+. Then, we will use as the integration profile Γ the image of the real interval $[-\pi/2, \pi/2]$. In formulas, the actual profile of integration that we use is parameterized as

$$\Gamma : x \mapsto (a_1 + a_2)\cos x + \mathrm{i}(a_2 - a_1)\sin x + A_3, \quad x \in \left[-\frac{\pi}{2}, \frac{\pi}{2}\right]. \tag{16}$$

In Figure 3 we show how z maps the horizontal strip $[-\pi/2, \pi/2] \times [-a, a]$ into the region limited by Γ_+ and Γ_-.

Let us focus first on the resolvent. In order to bound it, we will use a half-ellipse whose construction is described in Section 4.1. For the moment, we will resume its technical features (that we will use to prove the final error estimate) in the following assumptions.

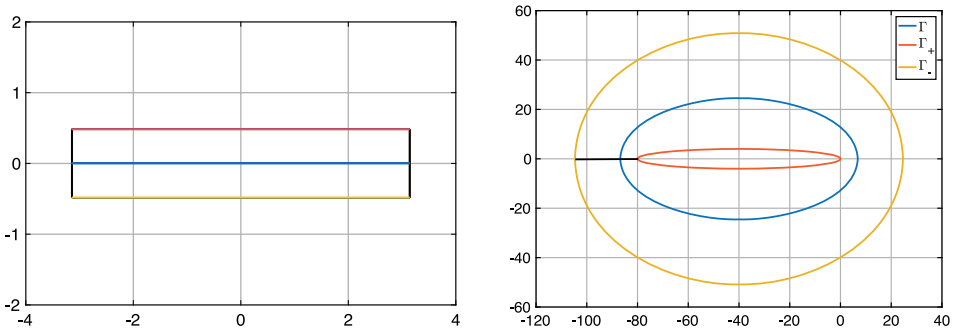

FIGURE 3. Action of the conformal mapping $z(w)$: it transforms horizontal segments in the complex plane (left) into ellipses (right).

Assumption 2. Assume that the matrix A and the time $t > 0$ are fixed. We assume that an ellipse $\tilde{\Gamma}$ of center $z_l \in \mathbb{R}$, axis along the coordinate directions, and right intersection with the real axis z_r is given in such a way that:

(1) its right half, that from now on we call Γ_+, leaves to its left the spectrum of A, $\sigma(A)$, and the set of the singularities of the function $\hat{b}$;
(2) $e^{z_l t} < \epsilon$, ϵ being the working precision.

Assumption 2.2 ensures that the integration ellipse (whose center will be z_l as well) is extended enough in the left half complex plane to make the values of the integrand function in (15) negligible when evaluated for points z on the ellipse of integration with $\Re(z) \approx z_l$. Basically the integrand function is "almost supported" in the half ellipse of integration.

Γ_+ is uniquely defined by z_l, z_r and the length of its vertical semiaxis S_v.

In general, an ellipse satisfying Assumption 2 for a given matrix A and vector $\hat{b}$ is not known a priori. Assume that a closed curve $\mathcal{C}$ surrounding the spectrum of A and the possible singularities of $\hat{b}$ is known. Moreover, we assume that $\mathcal{C}$ encloses the portion of the complex plane where the resolvent norm $\left\|(zI - A)^{-1}\right\|$ is large. Based on $\mathcal{C}$, a general algorithmic strategy for numerically computing Γ_+ is proposed in Section 4.1. Since for a general matrix A we do not have any information about its pseudospectral geometry, we approximate $\mathcal{C}$ by using `eigtool` [23]. The construction is general and does not require any a priori information about the spectral behaviour of A. Moreover, for the applications under consideration we show that a low resolution when approximating $\mathcal{C}$ might be enough for our purposes; see Section 4.2. Notice that if more information about the pseudospectral behaviour of A is available, the use of `eigtool` can be avoided.

Once Γ_+ is given, we want (13) to map the segment $[-\pi/2 + \mathrm{i}a, \pi/2 + \mathrm{i}a]$, for an a to be fixed, onto Γ_+. Imposing the ellipse $z(\cdot + \mathrm{i}a)$ to be centred at z_l, to pass through the point z_r, and to have vertical semiaxis of length S_v, we get

$$a_1 e^a + a_2 e^{-a} = z_r - z_l, \quad a_2 e^{-a} - a_1 e^a = S_v, \quad A_3 = z_l. \tag{17}$$

Solving (17) for a_1, a_2, A_3 we get

$$a_1 = \frac{e^{-a}}{2}\left(z_r - z_l - S_v\right), \tag{18}$$

$$a_2 = \frac{e^{a}}{2}\left(z_r - z_l + S_v\right), \tag{19}$$

$$A_3 = z_l, \tag{20}$$

which only depend on the real parameter a.

3.1. **Quadrature error estimates for the new integration contour.** Assume we are interested in approximating the unknown function u up to a certain precision that we call *tol*. Because of the presence of the exponential, we expect the integrand function G (15) to become smaller in modulus as z moves from the right to the left on the profile of integration. For this reason, we would like to truncate the integral once the function $|G|$ reaches the value *tol*. The motivation for fixing z_l as in point (2) of Assumption 2 is that we are assuming that the center of the half ellipse Γ_+ (that is, also the center of the integration ellipse Γ) is negative enough to make the integrand function close to the working precision at $z(\pi/2)$. In this way, for

every *tol* greater than the working precision, we can efficiently use the half-ellipse of integration Γ in order to recover approximations of the solution of order *tol*. In practice, we assume that there exists a *truncation parameter* $c \in]0, 1/2[$, defined as

$$|G(c\pi)| = tol\,. \tag{21}$$

The integrand we want to approximate is

$$I = \int_{-c\pi}^{c\pi} G(x)\,dx = u(t) + \mathcal{O}(tol).$$

In other words, we are neglecting not only the two half-lines of profile (4), but also the contribution to the integral coming from the portions of the ellipse parameterized in the intervals $[-\pi/2, -c\pi]$ and $[c\pi, \pi/2]$, as on these intervals the modulus of the integrand function is expected to be lower than the precision *tol* because of the rapidly decaying behaviour of the exponential. Applying the trapezoidal quadrature rule to I, we get the sum

$$I_N = \frac{c}{\mathrm{i}N} \sum_{j=1}^{N-1} e^{z(x_j)t} \left(z(x_j)I - A\right)^{-1} \Big(u_0 + \hat{b}(z(x_j))\Big)\, z'(x_j)\,, \quad x_j = -c\pi + j\frac{2c\pi}{N}.$$

We remark that, since the profile of integration is symmetric w.r.t. the real axis and $A \in \mathbb{R}^{n\times n}$, if $\hat{b}(\overline{z}) = \overline{\hat{b}(z)}$ the quadrature sum can be simplified to

$$I_N = \frac{2c}{N} \operatorname{Im}\left({\sum_{j=\lceil \frac{N}{2} \rceil}^{N-1}}' e^{z(x_j)t} \left(z(x_j)I - A\right)^{-1} \Big(u_0 + \hat{b}(z(x_j))\Big)\, z'(x_j) \right), \quad x_j = -c\pi + j\frac{2c\pi}{N}, \tag{22}$$

where the symbol $\sum'$ indicates that the term for $j = \lceil \frac{N}{2} \rceil$ ($x_j = 0$) is halved for N even.

From Theorem 1 we get the follow ing result.

Theorem 2. *Assume that the function* (15) *is analytic and bounded on the rectangle* $\left[-\frac{\pi}{2}, \frac{\pi}{2}\right] \times [-\mathrm{i}a, \mathrm{i}a]$ *for a certain* $a > 0$, *with* $z(w) = (a_1 + a_2)\cos w + \mathrm{i}\,(a_2 - a_1)\sin w + A_3$ *and* a_1, a_2, A_3 *given by* (18), (19), (20). *Assume, moreover, that the ellipse of integration has foci on the real axis. Set*

$$M_+ = \frac{1}{2\pi} \max_{x\in[-\pi/2,\pi/2]} \left| e^{z(x+\mathrm{i}a)t} \left(z(x+\mathrm{i}a)I - A\right)^{-1} \Big(u_0 + \hat{b}\left(z(x+\mathrm{i}a)\right)\Big)\, z'(x+\mathrm{i}a) \right|, \tag{23}$$

$$M_- = \frac{1}{2\pi} \max_{|x|\in[0,c\pi+c\pi/N]} \left| e^{z(x-\mathrm{i}a)t} \left(z(x-\mathrm{i}a)I - A\right)^{-1} \Big(u_0 + \hat{b}\left(z(!-\mathrm{i}a)\right)\Big)\, z'(x-\mathrm{i}a) \right|, \tag{24}$$

$$S_- = \frac{1}{2\pi} \max_{|x|\in[c\pi+c\pi/N,\pi/2]} \left| e^{z(x-\mathrm{i}a)t} \left(z(x-\mathrm{i}a)I - A\right)^{-1} \Big(u_0 + \hat{b}\left(z(x-\mathrm{i}a)\right)\Big)\, z'(x-\mathrm{i}a) \right|. \tag{25}$$

Finally, we assume that the integrand function $|G(w)| \le tol$ *for all* $w \in [-\pi/2, -c\pi] \cup [c\pi, \pi/2]$ *and take* N *large enough s.t.* $c(1 + 1/N) < 1/2$. *Then the quadrature*

error can be estimated by

$$err_N := |I - I_N| \leq \frac{2\pi c\left(1+\frac{1}{N}\right) M_- + 2(\pi/2 - c\pi - c\pi/N)S_- + \pi M_+}{e^{\frac{a}{c}N} - 1}$$

$$+4\left(\frac{\pi}{2} - c\pi + \frac{c\pi}{2N}\right) tol + \Delta \frac{2c\log 2}{N\pi} e^{\left(\left(a_1 e^{-a} + a_2 e^{a}\right)\cos(\pi/2-\delta)+A_3\right)t} \tag{26}$$

with $\|\hat{u}\left(z(\pi/2 - \delta \pm \mathrm{i}a)\right) z'(\pi/2 - \delta \pm \mathrm{i}a)\| \leq \Delta$ *and* δ *given by* (7) *(with* $\xi = c\pi$*).*

Proof. The result follows immediately from Theorem 1 with $\xi = c\pi$. Following the notation of Theorem 1, we set $B_+ = S_+ = M_+$ and $B_- = M_-$. In particular, we observe that $F(w) = e^{z(w)t}\hat{u}(z(w))z'(w)$ satisfies Assumption 1. Now, let us estimate $|F(\pi/2 - \delta + iy)|$ for $y \in [-a, a]$. We have

$$\left|e^{z(\pi/2-\delta+\mathrm{i}y)t}\hat{u}\left(z\left(\pi/2-\delta+\mathrm{i}y\right)\right) z'\left(\pi/2-\delta+\mathrm{i}y\right)\right| \leq \Delta e^{\left(\left(a_1 e^{y} + a_2 e^{-y}\right)\cos(\pi/2-\delta)+A_3\right)t}.$$

We observe that, from the hypothesis that both the foci are real, the horizontal semi-axis of the ellipse is longer than the vertical one, and so $a_1 + a_2 > a_2 - a_1$. Then a_1 is positive and so is a_2 (as from its definition in (19)). So, it is straightforward to prove that the maximum of the exponential is attained for $y = -a$. Indeed, consider the function $f(y) = a_1 e^{y} + a_2 e^{-y}$. Its derivative is $f'(y) = a_1 e^{y} - a_2 e^{-y}$ and it is positive if and only if

$$e^{2y} > \frac{a_2}{a_1}.$$

Recalling (18), (19) this reads as

$$e^{2y} > Ce^{2a},$$

where $C = \frac{z_r - z_l + r/\sin\tilde{y}}{z_r - z_l - r/\sin\tilde{y}} > 1$. Then, f is increasing if and only if $y > a + \frac{\log C}{2}$ and, since $y \in [-a, a]$, f attains its maximum for $y = -a$. □

Remark 2. In considering the term

$$B = \frac{2c\log 2}{N\pi} e^{\left(\left(a_1 e^{-a} + a_2 e^{a}\right)\cos(\pi/2-\delta)+A_3\right)t}, \tag{27}$$

we have that for $\delta \leq 2c\pi/N$, $\cos(\pi/2 - \delta) \to 0$ for $N \to \infty$. Moreover, as from equation (20), A_3 is chosen in order to have $e^{A_3 t}$ smaller than the working precision. In the end, we expect B to be much smaller than tol, at least for N large enough. In practice, B is very small (and negligible) also for very small values of N. To show this, we report in the following tables the size of the error B (27) that we observe in the numerical experiments displayed in Section 5. The term B, which is computed for $N = 5$, is much smaller than the accuracy tol in every case.

Black-Scholes

	$t = 1$		$t = 10$
$tol = 5e-3$	$1.1431e-18$	$tol = 5e-2$	$1.5555e-17$
$tol = 5e-6$	$4.8763e-18$	$tol = 5e-4$	$3.8418e-17$
$tol = 5e-9$	$4.1133e-14$	$tol = 5e-6$	$3.4109e-14$
$tol = 5e-11$	$1.6566e-17$	$tol = 5e-9$	$2.0858e-14$

Heston

	$t = 1$		$t = 10$
$tol = 5e-2$	$1.5409e-16$	$tol = 5e-2$	$2.8627e-16$
$tol = 5e-4$	$3.3070e-16$	$tol = 5e-4$	$5.7855e-14$
$tol = 5e-6$	$2.0416e-16$	$tol = 5e-5$	$1.3791e-16$
$tol = 5e-8$	$1.5943e-14$	$tol = 5e-6$	$3.7098e-12$

Remark 3. It is possible to select a positive ν and consider the trapezoidal rule with a quadrature step $(\pi+2\nu)/M$ for some natural number M, and to change the proof of Theorem 1 in order to make B as defined in (27), by evaluating the modulus of the integrand function along boundary of the rectangle $[-\pi/2,\pi/2]\times[-\mathrm{i}a,\mathrm{i}a]$.

In this way, the double exponential appearing in (27) vanishes because of the multiplication by $\cos(\pi/2)$, and the term B is even smaller. This change will make the length of the interval used to select the quadrature step dependent on the number of the nodes, and so it will no longer be possible to double this number saving the information computed on the previous nodes.

3.2. **Selection of the optimal integration contour.** Once a is fixed, the profile of integration Γ is uniquely defined by equations (18), (19), (20). To complete our construction, we need to ask the exponential part in the integrand G to be bounded on the external half ellipse $\Gamma_- = z\left([-\pi/2,\pi/2]\times\{-\mathrm{i}a\}\right)$. We have

$$e^{\mathrm{Re}(\zeta)t} \le e^{\mathrm{Re}(z(-\mathrm{i}a))} \quad \forall \zeta\in\Gamma_- .$$

Then, setting $z(-\mathrm{i}a)=D$, being $D>0$, we get that

$$e^{zt} \le e^{Dt} \quad \forall z\in\Gamma_- .$$

Using (13), (14), (15), we get

$$a_1 e^{-a} + a_2 e^{a} + A_3 = D \tag{28}$$

and, recalling equations (18), (19), (20), we get

$$D = \frac{e^{-2a}}{2}\left(z_r - z_l - \frac{r}{\sin\tilde{w}}\right) + \frac{e^{2a}}{2}\left(z_r - z_l + \frac{r}{\sin\tilde{w}}\right) + z_l. \tag{29}$$

The term D is made dependent on a so that it is not fixed *a priori* but it results from the optimization process of the parameter a. The construction summarized by the equations (18), (19), (20), (29) is still theoretical. In order to have it working, we need to find a parameter a (and, consequently, the truncation parameter c as defined in (21)) giving us the actual rate of convergence of the quadrature rule. We notice that the profile of integration z is given once a is fixed by formulas (18), (19). The tool we use to make the selection is the estimate (26). In order to simplify this estimate, we identify a leading term and neglect all the remaining ones, whose contribution is expected to be smaller. First of all, we notice that we expect $M_+ < M_-$ (defined in (23), (24)): this is due to the rapid decaying property of the exponential part in the integrand function, and, in practice, it holds in most cases. Moreover, we assume $S_- \ll M_-$ (where S_- is the one in (25)), since the exponential e^{zt} is larger for z parameterized in $[-c\pi, c\pi]$ than the one in $[-\pi/2,-c\pi]\cup[c\pi,\pi/2]$. In the end, we neglect the contribution of the term of order tol $\left(2\left(\frac{\pi}{2}-c\pi+\frac{2c\pi}{N}\right)tol\right)$, and the one of the term B (27) that is expected to be small (see Remark 2). Finally we simplify the error estimate (26) to

$$err_N \approx \frac{2\pi c M_-}{e^{\frac{a}{c}N}-1} . \tag{30}$$

Recalling (24), we roughly estimate $M_- \approx e^{Dt}$. Since we are interested in the order of magnitude of M_-, the estimate is precise enough for our purposes. In the end, within the accuracy, the quadrature error is

$$err_N \lesssim 2\pi c e^{Dt-\frac{a}{c}N} . \tag{31}$$

Assuming we seek approximation of $u(t)$ with a prescribed precision tol, we impose (31) to equal the precision. Solving for N, we compute

$$N = \frac{c}{a}\left(Dt - \log\left(\frac{tol}{2\pi c}\right)\right) \tag{32}$$

as the (theoretical) minimum number of quadrature nodes letting us reach the fixed accuracy. We aim to minimize N in order to make the convergence as fast as possible. The minimization of the function in (32) appears to be technically complicated since it depends on two variables (a, c), and the truncation parameter c depends on the profile of integration by the nonlinear constraint (21). For this reason, recalling that $c \leq 1/2$, we estimate

$$N = \frac{c}{a}\left(Dt - \log\left(\frac{tol}{2\pi c}\right)\right) \leq \frac{1}{2a}\left(Dt - \log\left(\frac{tol}{\pi}\right)\right). \tag{33}$$

The best that we can do to minimize N is to minimize the function

$$f(a) = \frac{1}{2a}\left(Dt - \log\left(\frac{tol}{\pi}\right)\right). \tag{34}$$

We fix an upper bound a_M and we seek minimizers of f in the interval $[0, a_M]$. In the numerical experiments we use $a_M = 1$. Once the minimizer value a has been computed, it uniquely defines the profile of integration by formulas (16), (18), (19), (20). Recall that D is a function of a by formula (29).

3.3. **Truncation error.** The profile (4) that we use to apply the Bromwich inversion formula is never used in practice: we just use a "small" portion of the ellipse contained in it. How much this portion is "small" depends on the fixed precision tol. In practice, we disregard all the points of (4) whose contribution is estimated to be smaller than tol. We resume the global error analysis in the following theorem.

Theorem 3. *Consider the integration profile defined in* (4)*, where the elliptical part* Γ *is constructed as in Section* 3.2*. We denote* ℓ_1, ℓ_2 *as in* (4)*, the parametrization of the two half-lines making part of* $\mathcal{G}$*, whose slope is assumed to be such that* $\mathcal{G}$ *encloses all the singularities of the integrand function. Moreover, assume that*

$$\|\hat{u}(z(x))z'(x)\| \leq K_\ell\,, \qquad \text{for } z(x) = \ell_1(x) \quad \text{and} \quad z(x) = \ell_2(x).$$

We assume that all the hypotheses of Theorem 2 *are satisfied. Then, the total error of our approximation of* (3) *is given by*

$$|u(t) - I_N| \leq err_N + err_T,$$

where err_N *is bounded by* (26) *and the truncation error* err_T *is bounded by*

$$|err_T| \leq K_\ell \frac{e^{z_l t}}{\pi t} + \left(\frac{1}{2} - c\right) tol$$

and does not depend on N*.*

Proof. Recall that we are approximating the integral

$$\frac{1}{2\pi \mathrm{i}} \int_{\mathcal{G}} e^{zt}\hat{u}(z)\,dz = \frac{1}{2\pi \mathrm{i}} \int_{-\infty}^{\infty} e^{z(x)t}\hat{u}(z(x))z'(x)\,dx,$$

with $z(x)$ defined by (4). First of all, we estimate the contribution of the two half-lines parameterized by the mappings ℓ_1 and ℓ_2. Choosing ℓ_1 as in (4), we have

(35)
$$\left|\frac{1}{2\pi \mathrm{i}}\int_{-\infty}^{-\frac{\pi}{2}} e^{\left(A_3+x+\frac{\pi}{2}-\mathrm{i}\left(A_2-d\left(x+\frac{\pi}{2}\right)\right)\right)t}\hat{u}(z(x))z'(x)\,dx\right| \leq \frac{K_\ell}{2\pi}\int_{-\infty}^{0} e^{A_3 t+xt}\,dx = K_\ell\frac{e^{z_l t}}{2\pi t},$$

with our choice $A_3 = z_l$ in (17). An analogous bound follows for $z(x) = \ell_2(x)$. We notice that the same estimate is not valid if we choose the two half-lines to be vertical.

Next we notice that the only portion of the ellipse that we approximate by using the quadrature formula (22) is the one parameterized on the interval $[-c\pi, c\pi]$. We now estimate the contribution of the other two intervals $[-\pi/2, -c\pi]$, $[c\pi, \pi/2]$. Recalling that we assume $|G(c\pi)| = tol$ and $|G(w)| \leq tol$ for all $w \in [-\pi/2, -c\pi] \cup [c\pi, \pi/2]$ as in Theorem 2, we have

$$\left|\frac{1}{2\pi \mathrm{i}}\int_{-\frac{\pi}{2}}^{-c\pi} e^{z(w)t}\hat{u}(z(w))z'(w)\,dw\right| \leq \frac{1}{2}\left(\frac{1}{2}-c\right)tol$$

and analogously for the integral on $[c\pi, \pi/2]$. In the end the error

$$\left|\frac{1}{2\pi \mathrm{i}}\int_{-c\pi}^{c\pi} e^{z(w)t}\hat{u}(z(w))z'(w)\,dw - I_N\right|,$$

where I_N is defined in (22), is estimated by Theorem 2. The thesis then follows. □

3.4. **Stability of the method.** One of the most attractive features of the method is its stability. In particular, we are able to compute the stability constant of the method.

In practice, we approximate the exact solution $u(t)$ by the linear combination

$$\tilde{I}_N = \frac{c}{N\mathrm{i}}\sum_{j=1}^{N-1} e^{z(x_j)t}\hat{u}_j z'(x_j), \tag{36}$$

where $\hat{u}_j = \hat{u}(z(x_j)) + \rho_j$ and ρ_j is the error in the numerical solution of the linear system

$$(z(x_j)I - A)\,\hat{u} = u_0 + \hat{b}(z(x_j)), \tag{37}$$

for x_j our quadrature nodes. We assume that the quadrature nodes x_j, the parametrization $z(x)$, and its derivative $z'(x)$ are computed exactly. We state the following result.

Proposition 1. *The described method is numerically stable and the stability constant is given by*

$$2a_2 c\, e^{(a_1+a_2+z_l)t}, \tag{38}$$

with a_1, a_2 given by formulas (18), (19).

Proof. The actual error in our computation is given by

$$e\tilde{r}r_N = \left|u(t) - \tilde{I}_N\right|.$$

We can estimate it in the following way:

$$e\tilde{r}r_N = \left| u(t) - \frac{c}{N\mathrm{i}} \sum_{j=1}^{N-1} e^{z(x_j)t} \hat{u}_j z'(x_j) \right| \leq err_N + err_T + err_N^{num},$$

with err_N and err_T as in Theorem 3 and

$$err_N^{num} = \left| \frac{c}{N\mathrm{i}} \sum_{j=1}^{N-1} e^{z(x_j)t} \left(\hat{u}(z(x_j)) - \hat{u}_j \right) z'(x_j) \right|.$$

Recalling that the integration contour Γ is parameterized as $z(x) = A_1 \cos x + \mathrm{i} A_2 \sin x + A_3$, with $A_1 = a_1 + a_2\,, A_2 = a_2 - a_1$ positive and $A_3 = z_l$, we have

$$\begin{aligned} err_N^{num} &\leq \frac{c}{N} \sum_{j=1}^{N-1} e^{(A_1 \cos x_j + A_3)t} |\rho_j|\, |-A_1 \sin x_j + A_2 i \cos x_j| \\ &\leq \frac{c}{N} \left(|A_1| + |A_2| \right) e^{(A_1+A_3)t} \rho N = c \left(A_1 + A_2 \right) e^{(A_1+A_3)t} \rho, \end{aligned}$$

where $\rho = \max_j |\rho_j|$. □

Remark 4. Given an integration contour Γ it is possible to compute the maximal precision we can get along Γ depending on the working precision,. First we compute the condition number of the matrix $z(x_j)I - A$, for a set of $x_j \in [-c\pi, c\pi]$. Then we use this information to estimate the numerical error ρ introduced when solving (37). At this point the computation of (38) is straightforward. We can incorporate this feasibility check in our algorithm, asking the user, in case the required precision is too high, to adjust the parameter *tol* by choosing a larger value.

3.5. **The approximation of the integrand tail.** Once the integration contour is computed, we need to approximate the truncation parameter c as defined in (21). Let us recast (21) into the system

$$Ke^{\mathrm{Re}(z(c\pi))t} = tol, \tag{39}$$

$$K = \frac{1}{2\pi} \left\| \hat{u}(z(c\pi)) z'(c\pi) \right\|. \tag{40}$$

Observe that, once the profile of integration is fixed, considering its parametrization $z(x) = A_1 \cos x + \mathrm{i} A_2 \sin x + A_3$, from (39) one has

$$c = \frac{1}{\pi} \arccos \left(\frac{1}{A_1 t} \log \left(\frac{tol}{K} \right) - \frac{A_3}{A_1} \right). \tag{41}$$

We suggest Algorithm 1 to iteratively compute c, K (where *prec* is the precision we ask for the constant K).

Algorithm 1: Numerical algorithm for approximating c, K.

Data: $K^{(1)}$ given, $K^{(0)} = K^{(1)} - 2prec$, $j = 0$
while $\left| K^{(j+1)} - K^{(j)} \right| \geq prec$ **do**
  $c^{(j)} = \frac{1}{\pi} \arccos \left(\frac{1}{A_1 t} \log \left(\frac{tol}{K^{(j)}} \right) - \frac{A_3}{A_1} \right)$;
  $K^{(j+1)} = \frac{1}{2\pi} \left\| \hat{u} \left(z(c^{(j)}\pi) \right) z'(c^{(j)}\pi) \right\|$;
  $j = j + 1$;

In all our numerical tests we observe that Algorithm 1 converges quickly to the sought values of c, K. We fix $prec = 10^{-1}$, and in at most $4-5$ iterations Algorithm 1 approximates the constant K with a precision approximately equal to 10^{-3}.

4. Practical implementation and computational cost

4.1. **Construction of the inner ellipse Γ_+.** In the described method, it is crucial to properly construct the inner ellipse Γ_+. It is conceived to bound the resolvent norm $\left\|(zI-A)^{-1}\right\|$ and it must be adjusted in order to leave to its left all the possible singularities of the vector $\hat{b}$. Let us focus, for the moment, on the resolvent norm: Γ_+ should be far enough from the spectrum of A but, if it's too far, it will produce a slowdown of the rate of convergence of the numerical scheme. For this reason, we decided to construct the ellipse by a procedure based on the computation of some pseudospectral level curve associated to the matrix A. Here we approximate these curves by using `eigtool` [23]. If some theoretical information about these curves is already known, we can skip the computation by `eigtool` and directly construct Γ_+ from it. An alternative approach to `eigtool` for the approximation of pseudospectral level sets has been developed in [16], where Newton's method is combined with an efficient computation of extremal singular values of possibly large and sparse matrices.

First of all, we define the region were we need to "place" our ellipse. This region is defined as $\{z \in \mathbb{C} \,|\, z_l \leq \mathrm{Re}(z) \leq z_r\}$, where z_l, z_r are real parameters to be chosen. This choice is partially heuristic and we ask the user to make a selection of these two values. We suggest the following criteria:

(i) Choice of z_l: once the time t is fixed, we need to have $e^{z_l t}$ smaller than the working precision. This is due to the fact that we use z_l as the center of the ellipse and, having in mind formula (35), we need to be sure that the contribution of the two lines of the profile (4) is negligible. In our experiments we choose $z_l \approx \frac{1}{t}\log(10^{-18})$.

(ii) Choice of z_r: this point is going to be the right intersection of our half-ellipse with the real axis. We can choose z_r as the rightmost intersection of the pseudospectral boundary $\partial\sigma_\varepsilon(A)$ with the real axis taking, for example, $\varepsilon = 10^{-9}$. In case $\hat{b}$ has some singularity to the right of this point, we need to move z_r as to be sure that all these singularities are to the left of the half ellipse. In our examples $\hat{b}$ has a singularity in the origin. For this reason we take z_r as a small positive number. Several values of z_r are tested in the numerical examples.

Now we need to estimate the resolvent norm in the strip $z_l < \mathrm{Re}(z) < z_r$. We do this by computing some suitable pseudospectral level curve of the matrix A. We recall that, given $\varepsilon > 0$, the ε-pseudospectral level curve of A is defined as

$$\sigma_\varepsilon(A) = \left\{ z \in \mathbb{C} \,:\, \left\|(zI-A)^{-1}\right\| = \frac{1}{\varepsilon} \right\}. \tag{42}$$

Moreover, we call a *weighted* ε-pseudospectral level curve as the set of points

$$\sigma_{\varepsilon,\omega}(A) := \left\{ z \in \mathbb{C} \,:\, e^{\mathrm{Re}(z)t}\left\|(zI-A)^{-1}\right\| = \frac{1}{\varepsilon} \right\}. \tag{43}$$

Let us fix two positive values $\varepsilon_1, \varepsilon_2$ (we use $\varepsilon_1^{-1}, \varepsilon_2^{-1}$ as bounding constants). We define $\mathcal{C}_1$ as the weighted ε_1-pseudospectral level curve and $\mathcal{C}_2$ the ε_2-pseudospectral

level curve. We compute $\mathcal{C}_1$, $\mathcal{C}_2$ in the strip $z_l < \mathrm{Re}(z) < z_r$. We notice that both $\mathcal{C}_1$, $\mathcal{C}_2$ are symmetric w.r.t. the real axis (and then we can just compute the two curves in the upper complex plane). For using our algorithm, we need the two level curves to be defined in the whole strip $\{z \in \mathbb{C} : z_l \le \mathrm{Re}(z) \le z_r\}$. For this reason, if it happens that for some $x \in [z_l, z_r]$ there is no $y \in \mathbb{R}$ such that $x + \mathrm{i}y$ is on the curve, we set $y = 0$ and we add the point x to the curve. After that, we define

$$\mathcal{C} = \{x + iy \in \mathbb{C} \,|\, x + \mathrm{i}y_1 \in \mathcal{C}_1 \,, x + \mathrm{i}y_2 \in \mathcal{C}_2 \text{ and } |y| = \max(|y_1|, |y_2|)\} \,. \tag{44}$$

We call $\mathcal{C}$ a *critical curve*. The meaning of the computation of $\mathcal{C}$ is the following: we approximate $\mathcal{C}_1$ in order to have a bound of $\left\| e^{zt} (zI - A)^{-1} \right\|$ and then of the integrand function (15), while on $\mathcal{C}_2$ we require that the norm of the resolvent is not too high in order to ensure that the condition number of the system (2) on the points of the curve Γ_+ (and then of the ellipse Γ) is not too large to cause a loss of accuracy. Defining $\mathcal{C}$ as in (44) will ensure that both the conditions are satisfied. From a practical point of view, we computed the value of the resolvent norm on a grid in the strip $z_l < \mathrm{Re}(z) < z_r$ using the Matlab code `eigtool`, [23]. It is straightforward to compute an approximation of $\mathcal{C}_1$, $\mathcal{C}_2$, and then $\mathcal{C}$ from it. In particular, we end up with a set of points $P_{\mathcal{C}} := \{x_i + \mathrm{i}y_i \,|\, y_i \ge 0 \,, i = 1, \ldots, m_{\mathcal{C}}\}$ approximating the upper part of the critical curve $\mathcal{C}$. The ellipse Γ_+ should be chosen in order to approximate in the sharpest way the curve $\mathcal{C}$. Moreover, since it may happen that the grid chosen by `eigtool` is too coarse, the critical curve may not capture some of the eigenvalues of A (in the case where the pseudospectral level curve near those are very small closed curves surrounding the eigenvalues). In addition, we also have to consider the possible singularities of $\hat{b}$ (that we assume to form a finite set). We call $\lambda_k + \mathrm{i}\eta_k$, $k = 1, \ldots, m_A$, the eigenvalues of A and $s_j + \mathrm{i}r_j$, $j = 1, \ldots, m_b$, the singularities of $\hat{b}$. Now define

$$\Phi = \{\rho_n + \mathrm{i}\sigma_n \,|\, n = 1, \ldots, m\} = P_{\mathcal{C}} \cup \sigma(A) \cup \{s_j + \mathrm{i}r_j \,|\, j = 1, \ldots, m_b\} \,.$$

The ellipse Γ_+ has to be chosen in order to enclose all the points of Φ. In practice, for the bounds

$$\begin{aligned} \left\| (zI - A)^{-1} \right\| &\le R_+ \qquad \text{for all } z \in \Gamma_+, \\ e^{\mathrm{Re}(z)t} \left\| (zI - A)^{-1} \right\| &\le W_+ \qquad \text{for all } z \in \Gamma_+ \end{aligned}$$

we set $W_+ = \varepsilon_1^{-1}$ and $R_+ = \varepsilon_2^{-1}$.

In order to compute Γ_+, let us identify $\mathbb{C}$ with $\mathbb{R}^2$. The interior of a general ellipse can be expressed by

$$\left\{x \in \mathbb{R}^2 \,|\, (x - \tilde{c})^T E (x - \tilde{c}) \le 1\right\}, \tag{45}$$

where $E \in \mathbb{R}^{2\times 2}$ is positive definite and $\tilde{c} = (z_l, 0)$ is the center of the ellipse (which is fixed). From Assumption 2 the axes of the ellipse are aligned with the coordinate directions. This implies that E is diagonal. Imposing that the ellipse passes through the point $(z_r, 0)$, we get $E_{1,1} = 1/(z_r - z_l)^2$. Now let us require that (45) is the minimal volume set containing all the computed points of Φ. To do that, let us write $E_{2,2} = 1/S_v^2$, with $S_v > 0$ being the length of vertical semiaxis. The minimal volume ellipsoid is recovered by minimizing S_v under the constraints

$$\frac{(x_1 - z_l)^2}{(z_r - z_l)^2} + \frac{x_2^2}{S_v^2} \le 1 \,, \quad (x_1, x_2) \in \Phi,$$

TABLE 1. Execution time for `eigtool`

Black-Scholes		Heston	
$t = 1$ Box $= [-40, 0.05] \times [-10, 10]$	15.251361 sec	$t = 1$ Box $= [-40, 0.09] \times [-10, 10]$	53.806976 sec
$t = 10$ Box $= [-4, 0.01] \times [-6, 6]$	15.523646 sec	$t = 10$ Box $= [-4, 0.06] \times [-6, 6]$	41.270690 sec

which leads to

$$S_v = \min_{(x_1,x_2)\in\Phi} \frac{|x_2|}{\sqrt{1 - \frac{(x_1-z_l)^2}{(z_r-z_l)^2}}}. \tag{46}$$

We would like to choose the right half of the boundary of the resulting ellipsoid as Γ_+. We observe that this boundary contains at least a point of Φ. If this point is an eigenvalue of A, Theorem 2 might not hold anymore (since the resolvent function fails to be analytic on Γ_+). To avoid this, instead of the original eigenvalues $\lambda_j = s_j + \mathrm{i}r_j$ $j = 1, \ldots, m$, we put in Φ the points

$$\tilde{\lambda}_j = s_j + \mathrm{i}(r_j + \nu),$$

ν being a small positive number ($\nu = 0.1$ for example). In this way the true eigenvalues λ_j will always be contained in the interior of the ellipsoid. Then, we choose Γ_+ as the right half-ellipse uniquely defined by z_l, z_r, and S_v computed by (46). With this choice, the hypothesis of Theorem 2 are always satisfied.

4.2. **Computational cost.** The method consists of two main parts: the *precomputing* part, where we construct the ellipse Γ_+ (see Section 4.1) and compute the actual ellipse of integration Γ (Section 3.1), and the *computing* part, where the quadrature formula (22) is applied to get the approximation of the unknown function $u(t)$. The precomputing part is essential in order to make the algorithm *general*, since by means of it all the pseudospectral information about the matrix A is approximated and, then, used to set the optimal profile of integration. In particular, in this part the software `eigtool` is employed. This software allows us to compute an approximation of the resolvent norm at the points of a rectangular grid in the complex plane. As a byproduct, `eigtool` also computes the eigenvalues of A. In Table 1, we report the time employed by `eigtool` in computing the approximations for both the Black–Scholes and Heston operators (the software is run on a laptop with a 2,4 GHz Intel Core i5 processor, using `Matlab R2016b`). In each case, we report the region of the complex plane (*Box*) where we seek the approximation. For Black–Scholes (size 200×200), the number of points defining the rectangular grid is set to 200, while it is set to 50 in the case of the Heston equation (size 2500×2500). The computation of the pseudospectral information is used to compute the critical curve $\mathcal{C}$ (44). The ellipse Γ_+ is selected by the algorithm explained in Section 4.1. We remark that the use of `eigtool` produces a larger computational cost w.r.t. other methods [11, 14, 15, 22]. However, we remark that these methods can be efficiently applied only if some pseudospectral information on A is already known. The choice of an algorithmic approach to investigate the behaviour of $\left\|(zI - A)^{-1}\right\|$

TABLE 2. Execution time for Black–Scholes.

	Select. Γ_+	Algorithm 1	Numerical quadrature	# Solved linear systems
$t = 1, tol = 5e-6$ $z_l = -40, z_r = 0.05$	0.6850 *sec*	0.0498 *sec* 4 iterations	0.1254 *sec*	34
$t = 10, tol = 5e-6$ $z_l = -4, z_r = 0.01$	0.3203 *sec*	0.0263 *sec* 4 iterations	0.1048 *sec*	34

TABLE 3. Execution time for Heston.

	Select. Γ_+	Algorithm 1	Numerical quadrature	# Solved linear systems
$t = 1, tol = 5e-6$ $z_l = -40, z_r = 0.09$	0.5360 *sec*	4.1404 *sec* 4 iterations	15.7459 *sec*	34
$t = 10, tol = 5e-6$ $z_l = -4, z_r = 0.06$	0.1315 *sec*	5.0225 *sec* 4 iterations	17.6780 *sec*	34

makes our method ready to be used for every system of ODEs of the form (1). In the case A is normal or some curve $\mathcal{C}$ bounding the region where the resolvent norm of A grows unboundedly is already known, the use of `eigtool` can be avoided.

For the computation of the truncation parameter c, we apply Algorithm 1. Every iteration of this procedure requires the evaluation of the function

$$\left\| (zI - A)^{-1} \left(u_0 + \hat{b}(z) \right) z' \right\| .$$

The cost of this evaluation depends on the size of A. We observe that for every iteration of Algorithm 1 the linear system

$$(\zeta I - A)\, \hat{u}(\zeta) = u_0 + \hat{b}(\zeta) \tag{47}$$

is solved for $\zeta = z(c\pi)$.

Concerning the integration part, i.e., the computation of the quadrature sum (22), the execution time depends on the size of the matrix A and the number of quadrature nodes that are used to get the desired accuracy. In order to save time, it is possible to precompute in parallel the integrand function at the quadrature nodes. Assuming the critical curve $\mathcal{C}$ already computed by `eigtool`, in Tables 2, 3 we report the time needed to select the profile Γ_+, to approximate the truncation parameter c by Algorithm 1 of Section 3.2 and to apply the quadrature sum (22) for $n = 30$ nodes. In all cases the resolution of the system (47) is done using the backslash command of Matlab. We also report the total number of solved linear systems.

We notice that it is possible to save the computation done for n when approximating the solution on $2n$ nodes (taking an extra node between each pair of consecutive points). In this way the execution time is halved, doubling the number of nodes.

An extra computational cost is needed for the *feasibility check*: it is possible, indeed, to approximate the stability constant of the method by computing the condition number of the system (37) for a set of points on the integration ellipse Γ, as explained in Section 3.4. However, this feasibility check can be skipped, and it is not necessary in order to run the algorithm even if it is useful to make a forecast

TABLE 4. CPU time for `eigtool` w.r.t. the number of grid points used.

Points	Execution time	Error w.r.t. reference solution
1000	247.435454 *sec*	0
500	60.914193 *sec*	$1.3927e-12$
250	18.149750 *sec*	0
100	4.917106 *sec*	0
50	2.684333 *sec*	$9.7751e-07$
25	2.675066 *sec*	$9.6867e-07$

on the maximal precision attainable on the computed Γ and to check whether the chosen tolerance is too sharp w.r.t. the working precision. It is worth noticing that the execution time needed to run `eigtool` strongly depends on the fixed number N of grid points. How to set this number? Numerical experiments suggest that we need a very low resolution of the computed pseudospectral level curves and the algorithm is robust w.r.t. the choice of N. For example, for the Black–Scholes case, with $t = 1$, $tol = 5 \cdot 10^{-6}$, we seek approximations of the resolvent norm in the box $[-40, 0.05] \times [-10, 10]$. Then, we compute a reference solution corresponding to $N = 1000$ and we measure the error w.r.t. this approximation of the solutions computed using $N = 500, 250, 100, 50, 25$. We also report the time employed by `eigtool` to perform the approximation. The results are listed in Table 4.

4.3. **Summary of the method.** The main parts of our method are: construction of the inner ellipse Γ_+, selection of the optimal integration contour Γ, and truncation of the profile Γ. In the end, the trapezoidal quadrature rule is applied to the selected portion of the ellipse to get the sought approximation of the solution to (1). For the sake of clarity, we briefly list the sequential steps which are needed to implement the method:

(1) Given A, b, and u_0 in (1), a time t, and a precision tol, the method provides an approximation of the unknown solution $u(t)$ of (1) with accuracy tol.
(2) Computation of the inner ellipse Γ_+. As explained in Section 4.1, the user is asked to choose the values of z_l, z_r (respectively, the center of Γ_+ and its right intersection with the real axis). This choice is partially heuristic but it is guided by (i), (ii) on page 1176. The procedure of Section 4.1 returns a point $d + \mathrm{i}r$ which uniquely defines the profile Γ_+, together with z_l, z_r. The construction uses `eigtool` for the computation of the pseudospectral sets $\sigma_{\varepsilon_2}(A), \sigma_{\varepsilon_1,\omega}(A)$ (as defined in (42), (43)). In all our numerical experiments we found the choices $\varepsilon_1 = 10^{-9}$, $\varepsilon_2 = 10^{-13}$ to be effective.
(3) Computation of the integration profile as explained in Section 3.2. In particular, the ellipse of integration is parameterized as

$$\Gamma: \quad z(x) = (a_1 + a_2)\cos x + \mathrm{i}(a_2 - a_1)\sin x + A_3,$$

with coefficients a_1, a_2, A_3 depending on just one free parameter a by formulas (18), (19), (20). In order to find the optimal profile of integration we minimize the scalar function of a in (34).
(4) Truncation of the Bromwich integral: since we are interested in approximating $u(t)$ within the precision tol, we only consider the portion of the

Bromwich integral parameterized in $[-c\pi, c\pi]$, for a certain truncation parameter c. The computation of c is performed by Algorithm 1 as explained in Section 3.2.

(5) Apply quadrature formula (22) to get the sought approximation of $u(t)$.

5. Numerical results

In this section, we collect some numerical results of our method. We first consider a canonical convection-diffusion equation, used as an academic test. We then test our approach with the Black–Scholes and Heston equations. The Black–Scholes model here is the same as the one considered in [11], while for the Heston model we consider a slightly different boundary condition from that in [11], following [7]. In all our numerical experiments we compute the absolute error w.r.t. a reference solution and use the standard Euclidean vector norm in $\mathbb{R}^n$. We show the absolute error rather than the relative error in order to check the match with the target accuracy *tol*.

Similarly to what is done in the other publications presented in the literature, we compute the error in the Cauchy problem while we do not address specific estimates of the spatial discretization error, which plays an important role in the considered PDEs. However, in deciding the error tolerances we take into account the order of magnitude of the discretization error, which is $\mathcal{O}(\Delta x^2)$ in the cases of Black and Scholes and Heston equations.

The function (34) is minimized by means of the built-in Matlab function `fminbnd`. In all the examples, we construct the inner ellipse Γ_+ as explained in Subsection 4.1, taking $\varepsilon_1 = 10^{-9}$, $\varepsilon_2 = 10^{-13}$.

5.1. **A canonical convection-diffusion operator.**

As a first illustration of our method we apply it, as in [22], to

$$u_t = u_{xx} + u_x\,, \quad t \geq 0\,, x \in [0, d], \tag{48}$$

with initial and boundary conditions

$$u(x,0) = 0\,, \quad u(0,t) = 0\,, \quad u(d,t) = 1\,, \quad t \geq 0,\ x \in [0,d]\,. \tag{49}$$

We consider $d = 400$ and follow the steps outlined in Section 4.3:

- Initial data: as done in [22], we discretize (48), (49) by a Chebyshev spectral method. The Chebyshev differentiation matrix used is of size 64×64. We fix $t = 1$, $tol = 5 \cdot 10^{-8}$.
- Computation of the inner ellipse Γ_+: following (i), (ii) of page 1176, we choose $z_l = -40$ and $z_r = 0.09$. We remark that in this case the vector b in (1) is constant and then $\hat{b}(z) = \frac{b}{z}$ has a singularity in the origin. For this reason, we must select $z_r > 0$. The procedure in Section 4.1 returns the point $d + \mathrm{i}r = -0.1071 + 0.3075\mathrm{i}$. The ellipse Γ_+ is plotted in Figure 4 together with the critical parabola in [22] ($x = -y^2$). The green line represents $\mathcal{C}$ in Section 4.1 and is computed by `eigtool`.
- Computation of the integration profile: once the parameters z_l, z_r, d, r are fixed, we minimize the function (34). It reaches its minimum at $a = 0.4543$. The minimization is done numerically by using the built-in MATLAB function `fminbnd`.

- Truncation of the Bromwich integral: we apply Algorithm 1 of Section 3.5 to compute the values of the truncation parameter c and the constant K defined by equations (39), (40). We fix $prec = 10^{-2}$ and $K^{(1)} = 100$. In three iterations Algorithm 1 computes $K = 0.2251$ and $c = 0.3160$.
- We apply quadrature formula (22). We apply it on n nodes, for $n = 5, \ldots, 30$. We compare the resulting approximation of $u(t)$ with the one computed by direct evaluation of the exponential matrix (`expm` function in Matlab). The results are plotted in Figure 4.

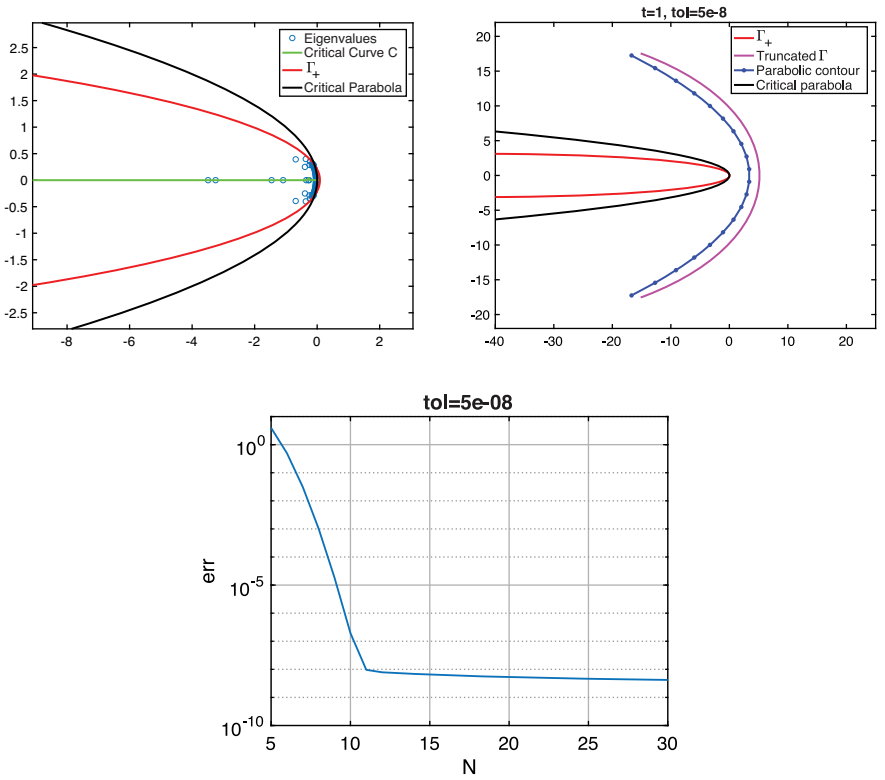

FIGURE 4. *Top Left:* comparison between Γ_+ and the theoretical critical parabola used in [22]. *Top Right:* plot of Γ_+ and truncated Γ. In green the critical parabola $x = -y^2$ and in blue the parabolic profile selected for $n = 10$ by the method [11]. *Bottom:* Error vs. number of nodes.

5.2. **Black–Scholes equation.** The well known (deterministic) Black–Scholes equation [2] has the following form:

$$\frac{\partial u}{\partial \tau} = \frac{1}{2}\sigma^2 s^2 \frac{\partial^2 u}{\partial s^2} + rs\frac{\partial u}{\partial s} - ru\,, \quad s > L\,, \quad 0 < \tau \leq t, \tag{50}$$

for L, t given, where the unknown function $u(s, \tau)$ stands for the fair price of the option when the corresponding asset price at time $t - \tau$ is s and t is the maturity time of the option. Moreover, $r \geq 0$, $\sigma > 0$ are given constants (representing the

interest rate and the volatility, respectively). In practice, for the sake of numerical approximation, we consider a bounded spatial domain, considering

$$L < s < S$$

for a sufficiently large S. We take (50) together with the following conditions, typical for the European option call:

$$u(s,0) = \max(0, s-K),$$

$$u(L,\tau) = 0\,, \quad 0 \le \tau \le t,$$

$$u(S,\tau) = S - e^{-r\tau}K\,, \quad 0 \le \tau \le t\,.$$

Following the same strategy adopted in [11], we discretize in space on a uniform space grid of $n = 200$ points in $[L, S]$, for $L = 0, S = 200$, using the classical centred finite difference scheme.

We choose $r = 0.06$, $\sigma = 0.05$, and $K = 80$. We plot the error for a selection of tolerances for the cases $t = 1$ and $t = 10$ (Figure 5).

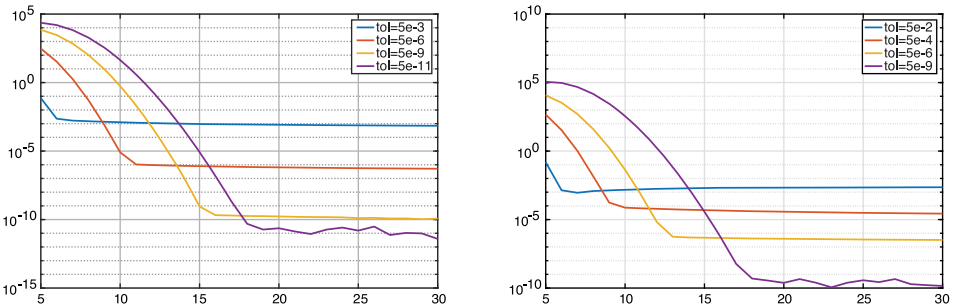

FIGURE 5. Error vs number of nodes for Black–Scholes. *Left:* $t = 1$ ($z_l = -40, z_r = 0.05$). *Right:* $t = 10$ ($z_l = -4, z_r = 0.01$).

5.3. **Heston equation.** The Heston equation [5] is

$$\frac{\partial u}{\partial \tau} = \frac{1}{2}s^2 v\frac{\partial^2 u}{\partial s^2} + \rho\sigma s v\frac{\partial^2 u}{\partial s \partial v} + \frac{1}{2}\sigma^2 v\frac{\partial^2 u}{\partial v^2} + (r_d - r_f)s\frac{\partial u}{\partial s} + \kappa(\eta - v)\frac{\partial u}{\partial v} - r_d u\,. \tag{51}$$

The unknown function $u(s, v, \tau)$ represents the price of a European option when at time $t - \tau$ the corresponding asset price is equal to s and its variance is v. We consider the equation on the unbounded domain

$$0 \le \tau \le t\,, \quad s > 0\,, v > 0,$$

where the time t is fixed. The parameters $\kappa > 0$, $\sigma > 0$, and $\rho \in [-1, 1]$ are given. Moreover, equation (51) is usually considered under the condition $2\kappa\eta > \sigma^2$ that is known as the Feller condition. We take equation (51) together with the initial condition

$$u(s, v, 0) = \max(0, s-K),$$

where $K > 0$ is fixed a priori (and represents the strike price of the option), and boundary conditions

$$u(L, v, \tau) = 0\,, \quad 0 \le \tau \le t\,.$$

For the numerical solution of (51), we need to choose a bounded domain of integration. In particular, we fix two positive constants S, V and we let the two variables s, v vary in the set

$$0 \le s \le S\,, \quad 0 \le v \le V\,.$$

On the new boundary, we need to add two more conditions (specific for the European call option),

$$\begin{aligned} &\frac{\partial u}{\partial s}(S, v, \tau) = e^{-r_f \tau}\,, \quad 0 \le \tau \le t, \\ &u(s, V, \tau) = s e^{-r_f \tau}\,, \quad 0 \le \tau \le t\,. \end{aligned} \tag{52}$$

The spatial discretization we adopted is the one introduced in [7]. We take $\kappa = 1.5, \eta = 0.04, \sigma = 0.3, \rho = -0.9, r_d = 0.025, r_f = 0, K = 100, L = 0, S = 8K, V = 5$. We plot the error for a selection of tolerances for the cases $t = 1$ and $t = 10$ (Figure 6).

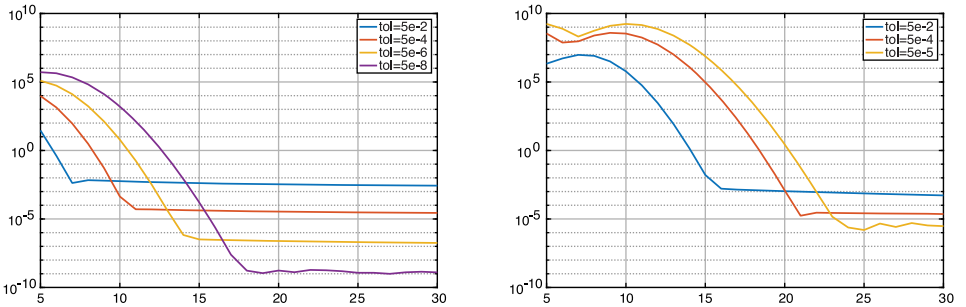

FIGURE 6. Error vs. number of nodes for Heston. *Left:* $t = 1$ ($z_l = -40, z_r = 0.09$). *Right:* $t = 10$ ($z_l = -4, z_r = 0.06$).

6. Comparison with other methods

6.1. **Comparison with parabolic contours.** A direct comparison with the method in [11] is not possible, since our algorithm works with the goal of a fixed accuracy while the one reported in [11] aims to reduce the error as N grows. Anyway, for the sake of comparison, we can run our algorithm as follows:

- for a set of target precisions ($tol = 10^{-1}, 10^{-2}, \ldots$ for example), we run our algorithm;
- for each tolerance we save the smallest number of quadrature nodes N for which tol is reached;
- for each tolerance we save the corresponding error $err(N)$.

Once we get the array $[N, err(N)]$, we can compare it with the corresponding error coming from the method of [11]. We make our experiments both for Black–Scholes and for Heston equations, for a selection of times t. In Figure 7 the comparison for Black–Scholes is depicted.

For the comparison in the case of the Heston equation, we recall that the boundary condition considered in [11] is slightly different from (52). However, the spectrum of the matrix A is quite similar, and thus we implement the method in [11] using the same inner parabola. Qualitatively, the numerical results we get for $t = 1$ are the same as the one in [11]. The comparison is showed in Figure 8.

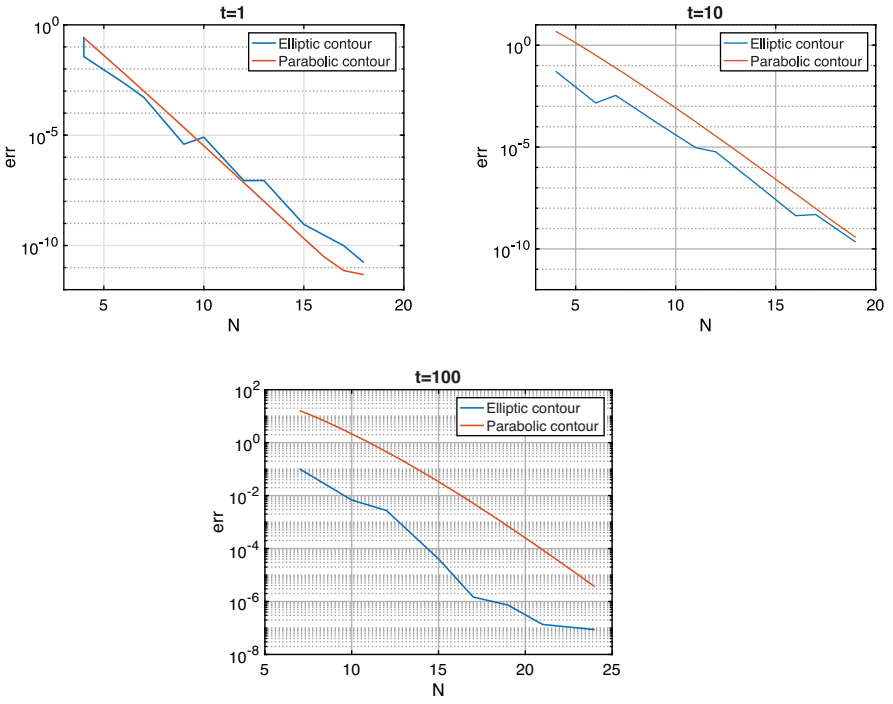

FIGURE 7. Black–Scholes equation, comparison between [11], and our method. *Top left:* $t = 1$, $z_l = -40$, $z_r = 0.05$. *Top right:* $t = 10$, $z_l = -4$, $z_r = 0.01$. *Bottom:* $t = 100$, $z_l = -0.5$, $z_r = 0.001$.

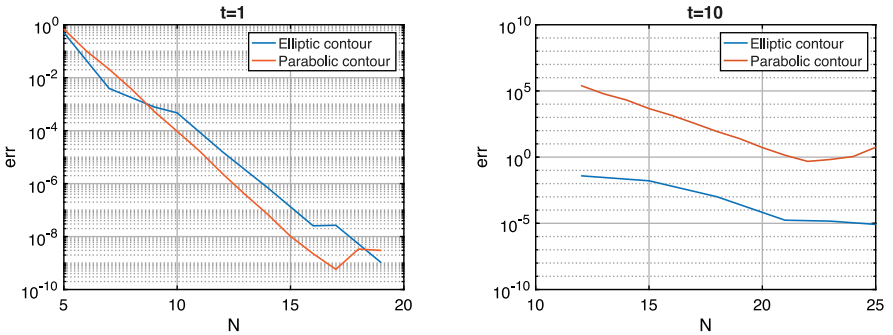

FIGURE 8. Heston equation, comparison between [11], and our method. *Left:* $t = 1$, $z_l = -40$, $z_r = 0.09$. *Right:* $t = 10$, $z_l = -4$, $z_r = 0.06$.

6.2. **Comparison with hyperbolic contours.** By using the same startegy as the previous subsection, we build the array $[N, err(N)]$. We compare these results with the method in [15] for both the cases of Black–Scholes and Heston equations. We set $\alpha = 0.4$, $d = 0.4$ as geometric parameters to bound the resolvent norm, as explained in [15]. This choice turns out to be effective and the method seems

to converge. However, in [15] no optimality criteria are given to select α, d, and they necessarily depend on the spectral geometry of A. Since [15] works on time intervals of the form $[t_0, \Lambda t_0]$, we provide a comparison for a selection of time ratios Λ and for the times $t = 1, 10$. The results are reported in Figures 9, 10, 11 and 12.

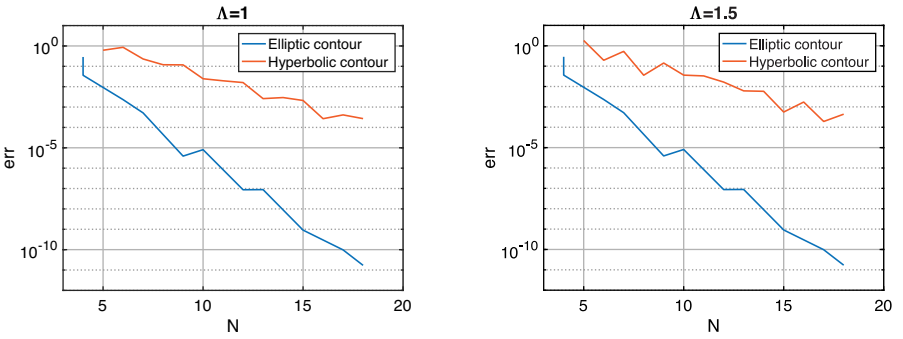

FIGURE 9. Black–Scholes equation, comparison between [15], and our method for $t = 1$ $z_l = -40$, $z_r = 0.05$. *Left:* $\Lambda = 1$. *Right:* $\Lambda = 1.5$.

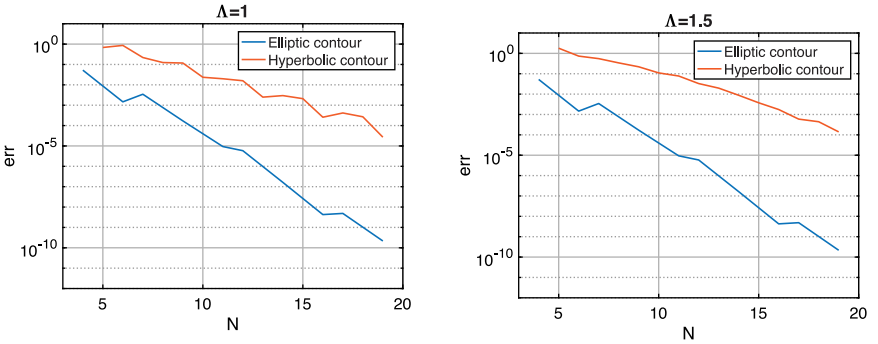

FIGURE 10. Black–Scholes equation, comparison between [15], and our method for $t = 10$ $z_l = -4$, $z_r = 0.01$. *Left:* $\Lambda = 1$. *Right:* $\Lambda = 1.5$.

7. Extension to the case of time intervals

We notice that the most expensive computation when evaluating (15) is the inversion of the matrix $zI - A$ at the quadrature nodes. This inversion does not involve the time t that appears only in the exponential part. For this reason, a great improvement to the efficiency of the method comes from the possibility of using a unique integration contour for a whole time interval $[t_0, t_1]$. In this section we suggest a strategy for computing a unique profile of integration, uniquely defined by the parameter a by (16), (18), (19), (20). By doing that, for a general time $t \in [t_0, t_1]$, we just need to compute the corresponding truncation parameter c and

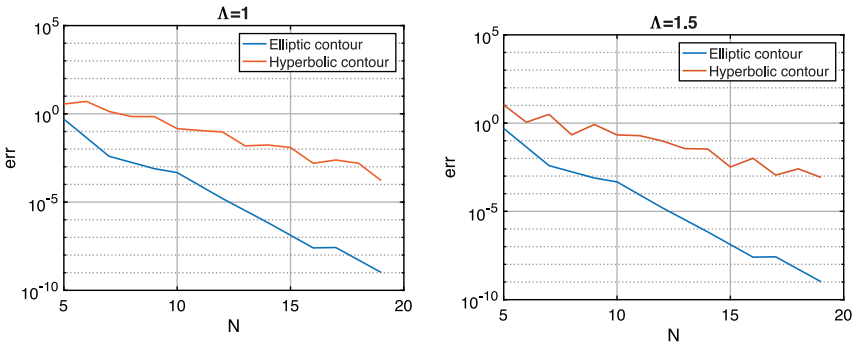

FIGURE 11. Heston equation, comparison between [15], and our method for $t = 1$ $z_l = -40$, $z_r = 0.09$. *Left:* $\Lambda = 1$. *Right:* $\Lambda = 1.5$.

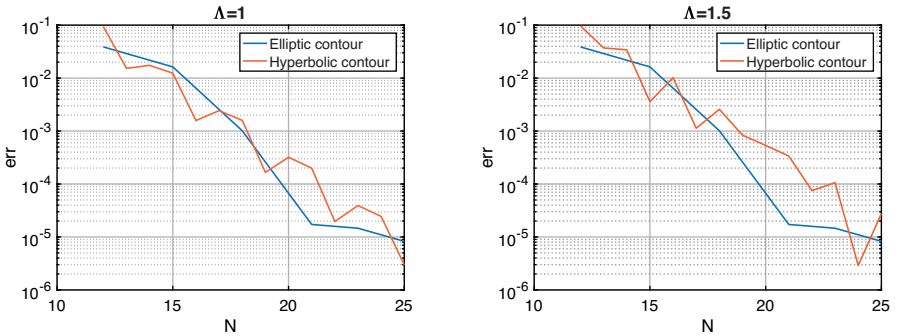

FIGURE 12. Heston equation, comparison between [15], and our method for $t = 10$ $z_l = -4$, $z_r = 0.06$. *Left:* $\Lambda = 1$. *Right:* $\Lambda = 1.5$.

the constant K in (39), (40). We would like to get an uniform error estimate like (30) for the whole interval $[t_0, t_1]$. Recalling (31) and the fact that $c \leq \frac{1}{2}$, we estimate

$$\sup_{t\in[t_0,t_1]} \|I_N - I\| \lesssim \pi e^{D(a)t_1} e^{-2aN}. \tag{53}$$

Using estimate (53), we recover the (theoretical) value of quadrature nodes sufficient to reach a prescribed precision *tol*. In particular, we get

$$N = \frac{1}{2a}\left(D(a)t_1 - \log\left(\frac{tol}{\pi}\right)\right). \tag{54}$$

Fix $t = t_0$. We construct Γ_+ as explained in Section 4.1 for the time t_0 (lower time of the interval). The choice of the smaller time t_0 reflects in the setting of the center of the integration ellipse z_l as explained in (i) of page 1176. In this way, we expect the contribution of the two half-lines in (4) to be negligible for all the times $t \in [t_0, t_1]$. An application of the construction of Section 4.1 gives the parameters

$z_l, z_r, d + \mathrm{i}r$ uniquely defining Γ_+. At this point, we minimize the function

$$f(a) = \frac{1}{2a}\left(D(a)t_1 - \log\left(\frac{tol}{\pi}\right)\right), \tag{55}$$

where $D(a)$ is given by (29). We end up with the optimal a defining uniquely the profile of integration by (16), (18), (19), (20). We will use this profile for every time $t \in [t_0, t_1]$.

Even if the profile of integration is the same for all times, when t changes we need to truncate it in a different point. For a general $t \in [t_0, t_1]$ we can compute the corresponding values c_t, K_t using Algorithm 1 of Section 3.5. In case we need to evaluate our integral for many times t, Algorithm 1 can be too expensive. Indeed, every iteration of this method requires the evaluation of the resolvent function. To save computational cost, we do as follows:

- we compute the pairs (c_0, K_0) and (c_1, K_1) corresponding to the times t_0, t_1;
- calling K_t the constant (40) for the general time $t \in (t_0, t_1)$ we make the assumption that K_t is linear, i.e., we assume that

$$K_t = K_0 + (K_1 - K_0)\frac{t - t_0}{t_1 - t_0}. \tag{56}$$

  The corresponding value of c_t is given by (41). This assumption turns out to be effective in the numerical experiments.

We show some numerical experiments for both Black–Scholes and Heston equations. Since the case of very large times is not really interesting (because the solution rapidly becomes stationary), we consider the case of intervals of the form $[t_0, \Lambda t_0]$ with $\Lambda = 10$. In particular, we make the experiments on the intervals $[0.1, 1]$, $[1, 10]$. In this way, we approximate the solution on the whole time interval $[0.1, 10]$ and the computation is competitive with respect to the classical PDEs integrators. In the plots of Figures 13, 14, we show the numerical results for Black–Scholes and Heston equations. The target tolerance we choose is $tol = 5 \cdot 10^{-8}$ for Black–Scholes and $tol = 5 \cdot 10^{-4}$ for Heston. We also fix $z_r = 0.01$ for Black–Scholes and $z_r = 0.06$ for Heston. A slowdown of the convergence rate as t decreases is observed. This

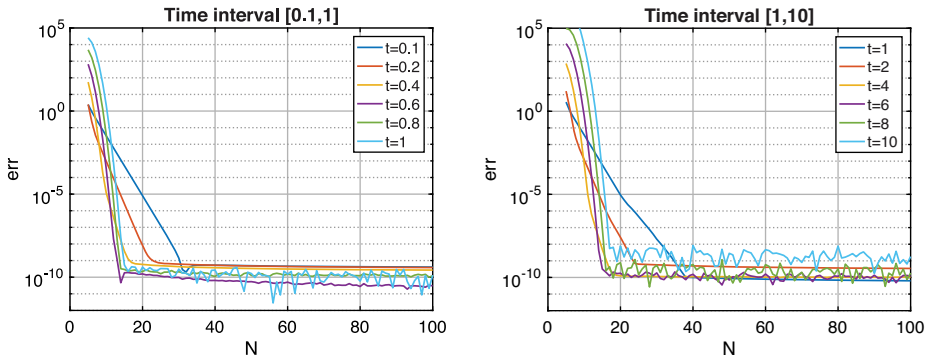

FIGURE 13. Black–Scholes equation, $tol = 10^{-8}$. *Left:* time interval $[0.1, 1]$, $z_l = -400$, $z_r = 0.01$. *Right:* time interval $[1, 10]$, $z_l = -40$, $z_r = 0.01$.

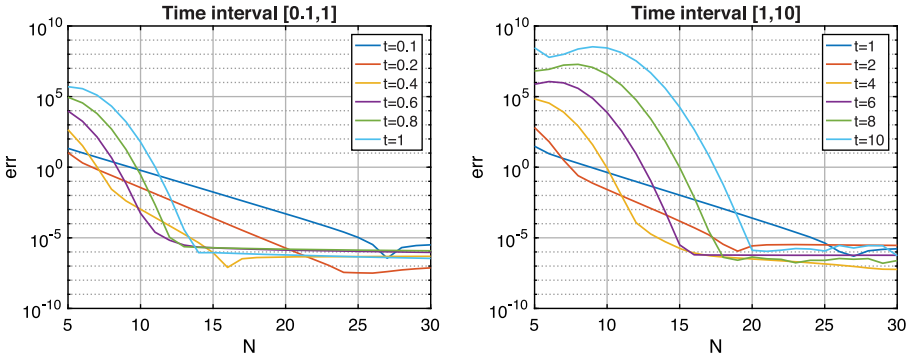

FIGURE 14. Heston equation, $tol = 10^{-4}$. *Left:* time interval $[0.1, 1]$, $z_l = -400$, $z_r = 0.06$. *Right:* time interval $[1, 10]$, $z_l = -40$, $z_r = 0.06$.

is due to the fact that c is decreasing w.r.t. time and the rate of convergence is $\mathcal{O}(e^{-\frac{a}{c}N})$. It is interesting to compare those performances with the one obtained by [15] since this method is also conceived to work on time intervals. In Figures 15, 16 the results are plotted (in both cases we take $\alpha = 0.4\,, d = 0.4$).

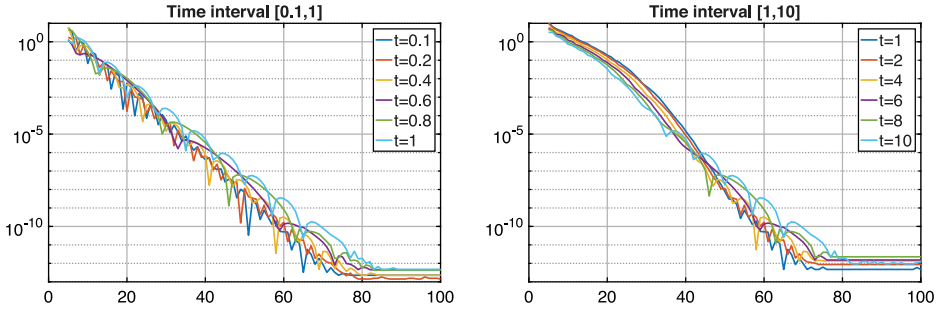

FIGURE 15. Black–Scholes equation using [15]. *Left:* time interval $[0.1, 1]$. *Right:* time interval $[1, 10]$.

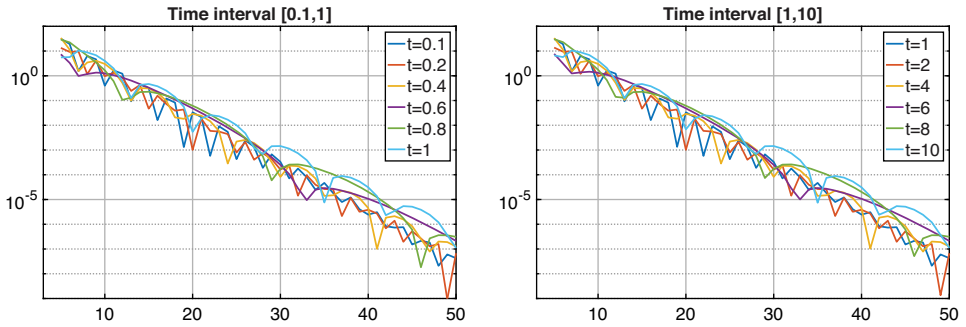

FIGURE 16. Heston equation using [15]. *Left:* time interval $[0.1, 1]$. *Right:* time interval $[1, 10]$.

8. Conclusions

In this paper we have proposed a new method for the numerical inversion of the Laplace transform of functions with specific properties arising in the space-time approximation of linear convection-diffusion equations.

Our method is based on a preliminary investigation of some pseudospectral level sets of A. In this way, the method can be directly applied to any linear system of ODEs with constant coefficient matrix, and no other a priori information about the matrix A is needed. This first step is not considered systematically in [11, 14, 15, 22]. In our applications, the computation of the pseudospectral level curves is performed by `eigtool`. The computational cost of the approximation made by using `eigtool` is reported in Subsection 4.2, where we also show that a low resolution in this approximation might be enough to construct a good integration contour.

We recap the main advantages of our method:

(i) It is designed in order to achieve a prescribed precision as fast as possible.

(ii) It is stable: adding quadrature nodes never deteriorates the quality of the approximation. As shown in [15] and [22], this can be a delicate issue in the numerical inversion of the Laplace transform.

The stability constant of the method can be computed to carry out an a priori feasibility check to detect if the prescribed accuracy is too high.

(iii) It is easily adapted to approximate the solution to (1) on relatively large time intervals of the form $[t_0, \Lambda t_0]$, with $\Lambda > 1$.

(iv) Once the target accuracy *tol* and the time t are fixed, our algorithm selects the profile of integration independently of the number of quadrature nodes. Thus, the cost of adding quadrature nodes to reach the target accuracy is low in comparison to the algorithms in [11, 15], where the integration contour does depend on the number of quadrature nodes.

Future research will be devoted to reducing the dependence on `eigtool`, which can be prohibitively expensive for large matrices arising from the spatial discretization of 2D and, specially, 3D convection-diffusion equations. The resolution of the linear systems with nonnormal matrices $zI - A$ should also be more carefully studied.

Acknowledgments

The authors thank the anonymous referee for constructive remarks and for suggesting the construction of the ellipse Γ_+ as it is now explained in Section 4.1. The authors also thank K. J. in 't Hout for providing the codes for implementing the method in [7].

References

[1] L. Banjai, M. López-Fernández, and A. Schädle, *Fast and oblivious algorithms for dissipative and two-dimensional wave equations*, SIAM J. Numer. Anal. **55** (2017), no. 2, 621–639, DOI 10.1137/16M1070657. MR3623208

[2] F. Black and M. Scholes, *The pricing of options and corporate liabilities*, J. Polit. Econ. **81** (1973), no. 3, 637–654, DOI 10.1086/260062. MR3363443

[3] B. Dingfelder and J. A. C. Weideman, *An improved Talbot method for numerical Laplace transform inversion*, Numer. Algorithms **68** (2015), no. 1, 167–183, DOI 10.1007/s11075-014-9895-z. MR3296705

[4] I. P. Gavrilyuk and V. L. Makarov, *Exponentially convergent parallel discretization methods for the first order evolution equations*, Comput. Methods Appl. Math. **1** (2001), no. 4, 333–355, DOI 10.2478/cmam-2001-0022. MR1892950

[5] S. L. Heston, *A closed-form solution for options with stochastic volatility with applications to bond and currency options*, Rev. Financ. Stud. **6** (1993), no. 2, 327–343, DOI 10.1093/rfs/6.2.327. MR3929676
[6] J. C. Hull, *Options, Futures and Other Derivatives*, 6th ed., Prentice Hall, New Jersey, 2006.
[7] K. J. in 't Hout and S. Foulon, *ADI finite difference schemes for option pricing in the Heston model with correlation*, Int. J. Numer. Anal. Model. **7** (2010), no. 2, 303–320. MR2587424
[8] K. J. in 't Hout, *ADI Schemes in the Numerical Solution of the Heston PDE*, Numerical Analysis and Applied Mathematics, eds. T. E. Simos et.al., AIP Conf. Proc: 936, 2007.
[9] K. J. in 't Hout and B. D. Welfert, *Stability of ADI schemes applied to convection-diffusion equations with mixed derivative terms*, Appl. Numer. Math. **57** (2007), no. 1, 19–35, DOI 10.1016/j.apnum.2005.11.011. MR2279504
[10] K. J. in 't Hout and B. D. Welfert, *Unconditional stability of second-order ADI schemes applied to multi-dimensional diffusion equations with mixed derivative terms*, Appl. Numer. Math. **59** (2009), no. 3-4, 677–692, DOI 10.1016/j.apnum.2008.03.016. MR2492284
[11] K. J. in 't Hout and J. A. C. Weideman, *A contour integral method for the Black-Scholes and Heston equations*, SIAM J. Sci. Comput. **33** (2011), no. 2, 763–785, DOI 10.1137/090776081. MR2785971
[12] M. Javed and L. N. Trefethen, *A trapezoidal rule error bound unifying the Euler-Maclaurin formula and geometric convergence for periodic functions*, Proc. R. Soc. Lond. Ser. A Math. Phys. Eng. Sci. **470** (2014), no. 2161, 20130571, 9, DOI 10.1098/rspa.2013.0571. MR3145072
[13] M. López-Fernández, C. Lubich, C. Palencia, and A. Schädle, *Fast Runge-Kutta approximation of inhomogeneous parabolic equations*, Numer. Math. **102** (2005), no. 2, 277–291, DOI 10.1007/s00211-005-0624-3. MR2206466
[14] M. López-Fernández and C. Palencia, *On the numerical inversion of the Laplace transform of certain holomorphic mappings*, Appl. Numer. Math. **51** (2004), no. 2-3, 289–303, DOI 10.1016/j.apnum.2004.06.015. MR2091405
[15] M. López-Fernández, C. Palencia, and A. Schädle, *A spectral order method for inverting sectorial Laplace transforms*, SIAM J. Numer. Anal. **44** (2006), no. 3, 1332–1350, DOI 10.1137/050629653. MR2231867
[16] G. Nino, *Laplace transform methods based on pseudospectral roaming for convection-diffusion equations*, PhD thesis, Gran Sasso Science Institute, L'Aquila, 2017.
[17] S. C. Reddy and L. N. Trefethen, *Pseudospectra of the convection-diffusion operator*, SIAM J. Appl. Math. **54** (1994), no. 6, 1634–1649, DOI 10.1137/S0036139993246982. MR1301275
[18] D. Sheen, I. H. Sloan, and V. Thomée, *A parallel method for time discretization of parabolic equations based on Laplace transformation and quadrature*, IMA J. Numer. Anal. **23** (2003), no. 2, 269–299, DOI 10.1093/imanum/23.2.269. MR1975267
[19] A. Talbot, *The accurate numerical inversion of Laplace transforms*, J. Inst. Math. Appl. **23** (1979), no. 1, 97–120. MR526286
[20] L. N. Trefethen and M. Embree, *Spectra and Pseudospectra*: *The Behavior of Nonnormal Matrices and Operators*, Princeton University Press, Princeton, NJ, 2005. MR2155029
[21] L. N. Trefethen and J. A. C. Weideman, *The exponentially convergent trapezoidal rule*, SIAM Rev. **56** (2014), no. 3, 385–458, DOI 10.1137/130932132. MR3245858
[22] J. A. C. Weideman, *Improved contour integral methods for parabolic PDEs*, IMA J. Numer. Anal. **30** (2010), no. 1, 334–350, DOI 10.1093/imanum/drn074. MR2580562
[23] Thomas G. Wright, EigTool, http://www.comlab.ox.ac.uk/pseudospectra/eigtool/, 2002.

Gran Sasso Science Institute, via Crispi 7, L'Aquila, Italy
Email address: nicola.guglielmi@gssi.it

Departamento de Análisis Matemático, Estadística e I.O., Matemática Aplicada, Facultad de Ciencias, Universidad de Málaga, Campus de Teatinos s/n, 29080, Málaga, Spain; and Department of Mathematics Guido Castelnuovo, Sapienza University of Rome, Italy
Email address: maria.lopezf@uma.es

Section de Mathématiques, Université de Genève, 2-4 rue du Lièvre, 1211 Genève, Switzerland
Email address: giancarlo.nino@unige.ch